ADVANCED FUNCTIONAL MATERIALS
www.afm-journal.de

Stoichiometry Variation in Materials with Three Mobile Carriers—Thermodynamics and Transport Kinetics Exemplified for Protons, Oxygen Vacancies, and Holes

D. Poetzsch, R. Merkle, and J. Maier*

Dedicated to Prof. Klaus Funke on the occasion of his 70th birthday.

Materials with three independent mobile charge carriers, in the sense of not being in local defect-chemical equilibrium though naturally coupled through electroneutrality, are encountered in various cases of scientific and technological relevance. Examples are proton conducting perovskites under conditions at which hole and also oxygen vacancy conductivity may become significant, and mixed conducting cathode materials suited for fuel cells using proton conducting oxide electrolytes. Already the thermodynamics of the equilibrium situation is complex as a p_{H_2O} increase can lead to proton incorporation by water uptake (pure acid–base reaction) or by hydrogenation (redox reaction). As far as the even more complex transport kinetics are concerned, diffusion equations are derived which are exact for the interaction-free (ideally dilute) situation. Kinetic implications are discussed and checked by exemplary numerical simulations. The treatment includes simple sub-cases such as one-fold relaxation on p_{H_2O} change, as well as complex patterns characterized by the appearance of more than one characteristic time scales ("twofold relaxation") or apparent "moving boundary" kinetics. Implications for stability and functionality of ceramic materials are discussed.

1. Introduction

It is a key characteristic of many functional materials that they contain mobile ionic and frequently also electronic carriers.[1] This specific feature forms the link between chemical and electrical properties and is hence decisive for electrochemistry and electrochemical devices such as batteries, fuel cells, or electrochemical sensors. The vast majority of functional materials are not binary. Even if one ionic component is overwhelmingly responsible for the ionic conductivity, this finite mobility of a further component leads to serious, typically unwanted long-time effects.[2] There are various situations where two ionic species can be similarly conductive, e.g., in proton conducting oxides. Though there the peculiarities appear in a most striking form and can be easily experimentally measured, the treatment to be outlined is general. It is generally accepted that the definition of stoichiometry is crucial for defining the charge carrier concentrations. The process of stoichiometry variation and hence of chemical diffusion addressed here is thus of substantial interest from an applied (e.g., tuning material properties by fine-tuning oxygen nonstoichiometry, or serving as operation principle in highly selective gas sensors), from a methodological (diffusion experiments used as a tool to investigate defect chemistry and transport), as well as from a fundamental point of view.

In ionic solids, chemical diffusion proceeds by ambipolar transport of charged carriers (point defects) driven by chemical potential gradients of the neutral components.[3,4] Many chemical diffusion processes can be described by a single chemical diffusion coefficient which comprises contributions from either one ion sort and electronic carriers (e.g., chemical diffusion of oxygen)[3,4] or two ion sorts (e.g., chemical diffusion of water).[5,6] This also holds if the number of defect sorts is larger provided they are internally in defect-chemical equilibrium, e.g., via Frenkel or band–band reaction, and even holds if fast internal reactions complicate the picture.[7] However, in systems with more than two mobile carriers which are not locally in mutual equilibrium, unusual relaxation kinetics have been observed, e.g., in TiO_2 and donor-doped $BaTiO_3$ with contributions from electrons, cation defects, and oxygen vacancies,[8,9] or in acceptor-doped perovskites such as Fe-doped $SrTiO_3$ or $Sr(Ce,Yb)O_{3-\delta}$ where p_{H_2O} changes can result in strong transient concentration changes of electronic carriers.[10–13] Depending on the material and the measured quantity (conductivity, weight change, etc.) this behavior can lead to monotonic change of the measured property but obviously with two different time constants,[8,9] or even to a peculiar nonmonotonic behavior where the regimes with different time constants are separated by a minimum or maximum in the measured quantity.[10–13] In situ space-resolved optical spectroscopy provided a clear picture of the local nonstoichiometry as it yields space-resolved concentration profiles, rather than integral values.[10]

It is also noteworthy that the complex diffusion kinetics in these cases are not a consequence of applying extremely large driving forces (which is known to lead to deviations from

Dr. D. Poetzsch, Dr. R. Merkle, Prof. J. Maier
Max Planck Institute for Solid State Research
Stuttgart, Germany
E-mail: r.merkle@fkf.mpg.de

DOI: 10.1002/adfm.201402212

simple diffusion profiles caused by the dependence of the chemical diffusion coefficient on local stoichiometry)[14] but occur even for small changes in component activity. Rather, it is related to the fact that such systems exhibit an additional degree of freedom. In contrast to materials with only two mobile carriers (the concentrations of which are directly coupled to each other by the electroneutrality condition), the electroneutrality condition must here be fulfilled within an ensemble of three carriers, which breaks up the direct coupling of the carrier concentrations. This allows a fast carrier species to respond to an external driving force without being "delayed" by the motion of the slowest species in the system, because electroneutrality will be fulfilled by (transient) concentration changes of one other comparably fast carrier. Since many materials properties such as conductivity depend on point defect concentrations, this has direct consequences for the materials properties.

Substantial contributions to this field have been delivered by the group of Yoo.[8,9,11] Our work goes beyond that treatment in deriving exact diffusion laws as we will set out below. The exhaustive treatment though focusing on dilute and interaction-free conditions will allow us to precisely model the three-carrier situation numerically for a variety of conditions.

To be specific, let us consider oxides with mixed conductivity of protons $OH_O^{\bullet}$,[15b] oxygen vacancies $V_O^{\bullet\bullet}$, and electron holes $h^{\bullet}$, which recently gained perceptible interest, as they are key functional materials (ceramic hydrogen permeation membranes,[16–18] electrolytes,[13,20] and electrode materials[15] for protonic ceramic fuel cells H-SOFC). In such perovskites, the peculiar "twofold" kinetics was interpreted as a decoupling of normally simultaneously occurring diffusion processes of these two carriers (despite their different mobilities) which together constitute the overall stoichiometry change demanded by the experiment. It is the presence of mobile electronic defects as a third carrier that leads to an approximately independent chemical diffusion of H and O. This is qualitatively illustrated in **Figure 1** where for high hole concentration the ambipolar diffusion of water ($V_O^{\bullet\bullet}$ directly coupled to $OH_O^{\bullet}$) is replaced by a sequence of fast hydrogen diffusion and subsequent slower oxygen diffusion. While the overall reaction is the same as for the onefold relaxation, intermediately the sample is in a reduced state with transiently greatly decreased $h^{\bullet}$ concentration (corresponding to a nonmonotonic behavior of $[h^{\bullet}]$ in the course of the relaxation process). This situation is similar to the formation of intermediates in reaction kinetics the presence of which is of relevance for the reaction rate. Related phenomena where a gradient in one component can lead to an "uphill diffusion" of another component were observed in the context of $V_O^{\bullet\bullet}/OH_O^{\bullet}/h^{\bullet}$ conducting permeation membranes under simultaneous p_{H_2O} and p_{O_2} gradients.[16–18]

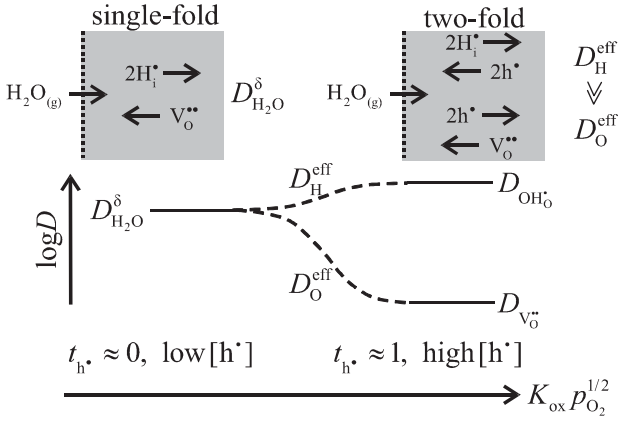

Figure 1. Possible stoichiometry relaxation processes upon p_{H_2O} increase in the gas phase (grey: bulk of the sample; dotted line: surface, assumed to have sufficiently fast exchange reaction with the gas phase), adapted from a previous study.[15] An experimental example for the transition from onefold to twofold kinetics for $BaZr_{0.8}Y_{0.2}O_{3-\delta}$ (varying p_{O_2} over several orders of magnitude) is given in the literature.[13]

In the present article, first the equilibrium thermodynamic situation is analyzed, then the theoretical framework for diffusion kinetics with three carriers involved is set out, and finally selected numerical results are discussed. The analysis based on irreversible thermodynamics will be shown to give exact diffusion coefficients for ideally dilute situations. The results reproduce the limiting cases shown in Figure 1, and agree with the ad hoc assumptions of Yu et al.[10] (but partly disagree with analyses found in the literature).[11,13] All analytical results are backed up by exemplary numerical simulations, which cover a range of materials ranging from electrolyte-related oxides with comparably low $h^{\bullet}$ concentration to mixed $V_O^{\bullet\bullet}/OH_O^{\bullet}/h^{\bullet}$ conductors with high $h^{\bullet}$ concentration (all computational details are given in Appendixes 1–3). Even for conditions which lead to perceptible decoupling of H and O diffusion a set of two chemical diffusion coefficients is not sufficient to correctly describe the system. The results also explain naturally the observation of a "moving boundary" phenomenon that otherwise has to be invoked in the simple decoupled picture (cf. Fe-doped $SrTiO_3$ in the literature).[12] Part II[19] will explore the relations between the degree of decoupling and several material parameters, and investigate also relaxations after p_{O_2} changes.

To be precise in terminology we will use the term two-component diffusion to describe the general case (diffusion of H and O, which degenerates to single component diffusion, e.g., H_2O, under special conditions). The two-component diffusion can be more or less decoupled as outlined above. We use the term twofold kinetics whenever we explicitly exclude the single-component case. Furthermore, we assume the equilibration with changes component activities to be diffusion-controlled, i.e., imply sufficiently fast surface exchange reactions.

2. Equilibrium Thermodynamics

Before we come to the main discussion of the diffusion kinetics, we first have to consider the equilibrium situation. The phenomena arising when three carriers are involved in defect chemistry and transport kinetics are analyzed in the present study for an oxide characterized by oxygen vacancies $V_O^{\bullet\bullet}$ and protons $OH_O^{\bullet}$ as ionic defects and electron holes $h^{\bullet}$ as electronic defect (typical for perovskite proton conductors and mixed $V_O^{\bullet\bullet}/OH_O^{\bullet}/h^{\bullet}$ conductors in an extended p_{O_2} range).[10,13] The equilibration of such a material can be expressed by the oxygenation reaction (square brackets denote concentrations given as molar fraction; assuming ideally dilute situation)

$$1/2O_2 + V_O^{\cdot\cdot} \rightleftharpoons O_O^x + 2h^{\cdot} \quad K_O = \frac{[O_O^x][h^{\cdot}]^2}{p_{O_2}^{1/2}[V_O^{\cdot\cdot}]} \tag{1}$$

and the hydration reaction

$$H_2O + V_O^{\cdot\cdot} + O_O^x \rightleftharpoons 2OH_O^{\cdot} \quad K_W = \frac{[OH_O^{\cdot}]^2}{p_{H_2O}[O_O^x][V_O^{\cdot\cdot}]} \tag{2}$$

describing water uptake. Equation (1) is a redox reaction, while Equation (2) is a pure acid–base reaction. The combination of both reactions results in proton uptake at the expense of holes

$$H_2O + 2O_O^x + 2h^{\cdot} \rightleftharpoons 2OH_O^{\cdot} + 1/2O_2 \quad K_{W/O} = \frac{p_{O_2}^{1/2}[OH_O^{\cdot}]^2}{p_{H_2O}[O_O^x]^2[h^{\cdot}]^2} \tag{3}$$

This hydrogenation reaction conveniently describes the dominating process in various materials and conditions, nevertheless one of the three reactions is redundant ($K_{W/O}=K_W/K_O$). Defect concentrations for given $K_O p_{O_2}^{1/2}$ and $K_W p_{H_2O}$ are calculated numerically considering the electroneutrality condition $[A'] = 2[V_O^{\cdot\cdot}] + [OH_O^{\cdot}] + [h^{\cdot}]$ with acceptor concentration $[A']$ and oxygen site balance which in the case of perovskites reads $3 = [O_O^x] + [V_O^{\cdot\cdot}] + [OH_O^{\cdot}]$, see Appendix 1.

According to the above equations, the defect concentrations can be varied by the partial pressures p_{H_2O} and p_{O_2} as well as by the mass action constants K_O, K_W (changing temperature or the thermodynamic parameters $\Delta H_O^0, \Delta S_O^0, \Delta H_W^0, \Delta S_W^0$ of reactions (1) and (2), i.e., changing the material). The defect concentrations $[V_O^{\cdot\cdot}]$, $[OH_O^{\cdot}]$, and $[h^{\cdot}]$ within an extended range of $K_O p_{O_2}^{1/2}$ and $K_W p_{H_2O}$ values are shown in **Figure 2**. Different regions corresponding to characteristic material properties can be distinguished. P-type electronic conductors with negligible ionic conductivity are located in the right corner. In the hind corner (low $K_O p_{O_2}^{1/2}$ as well as $K_W p_{H_2O}$ values) we find materials with high oxygen vacancy but negligible proton and hole concentrations, i.e., $V_O^{\cdot\cdot}$-conducting electrolytes, while proton-conducting electrolytes are located in the left corner. A decrease of $K_W p_{H_2O}$ which can be caused by (i) increasing the temperature (ΔG_W^0 becoming less negative owing to the negative ΔS_W^0), (ii) decreasing p_{H_2O}, (iii) modifying the materials chemistry (typically, ΔH_W^0 becoming less negative for less basic materials)[20,21] leads to dehydration and transforms the proton conductor eventually into a $V_O^{\cdot\cdot}$ conductor. Starting from the hind corner, an increase of $K_O p_{O_2}^{1/2}$ (making ΔH_O^0 more negative by introducing redox-active cations)[22,23] leads to mixed $V_O^{\cdot\cdot}/h^{\cdot}$ conductors which are desired, e.g., as cathode materials on $V_O^{\cdot\cdot}$-conducting electrolytes. Finally, a combined increase of $K_O p_{O_2}^{1/2}$ and $K_W p_{H_2O}$ in the front corner leads to mixed $OH_O^{\cdot}/h^{\cdot}$ conducting materials (with possibly some $V_O^{\cdot\cdot}$ conductivity).

Even for materials with low redox activity such as $Ba(Ce,Zr,Y)O_{3-\delta}$ the combination of high p_{O_2} and low hydration can result in a perceptible hole transference number.[24,25] This can lead to severe complications in the interpretation of electrochemical oxygen reduction kinetics measurements in gas-symmetrical cells.[26] On the other hand, mixed $OH_O^{\cdot}/h^{\cdot}$ conductors with reasonably high electronic conductivity are desired as cathode materials in H-SOFC[15,27] allowing one to extend the reaction zone for oxygen reduction. Finding such materials can be a challenge because $[h^{\cdot}]$ and $[OH_O^{\cdot}]$ behave antagonistically. The positive defects compete in the electroneutrality condition (Figure 2: high concentrations of one defect lead to a decrease of the other two positive defect concentrations). In addition, an increased $[h^{\cdot}]$ corresponding to a high oxidation state or redox-activity of transition metals decreases the basicity of the material (decreasing the effective negative charge density of the oxide ions by more covalent metal–oxygen bonding character), making hydration less favorable. A variation of the cation composition to increase K_O will tend to decrease K_W, resulting in nonidealities in the defect chemical behavior. This antagonistic behavior shows up in $La_{0.6}Sr_{0.4}(Sc,Fe)O_{3-\delta}$ perovskites for which already the introduction of 5% Fe drastically decreases the proton uptake.[28]

The thermodynamic response of a material to changes of p_{O_2} (at constant p_{H_2O}) or p_{H_2O} (at constant p_{O_2}) can be expressed via chemical capacitances (inversely proportional to the thermodynamic factor), normalized to sample volume[29]

$$C_O^{\delta} \equiv 4F^2 \frac{\partial c_O}{\partial \mu_O} = -8F^2 \frac{\partial [V_O^{\cdot\cdot}]}{RT\, \partial \ln p_{O_2}} \tag{4}$$

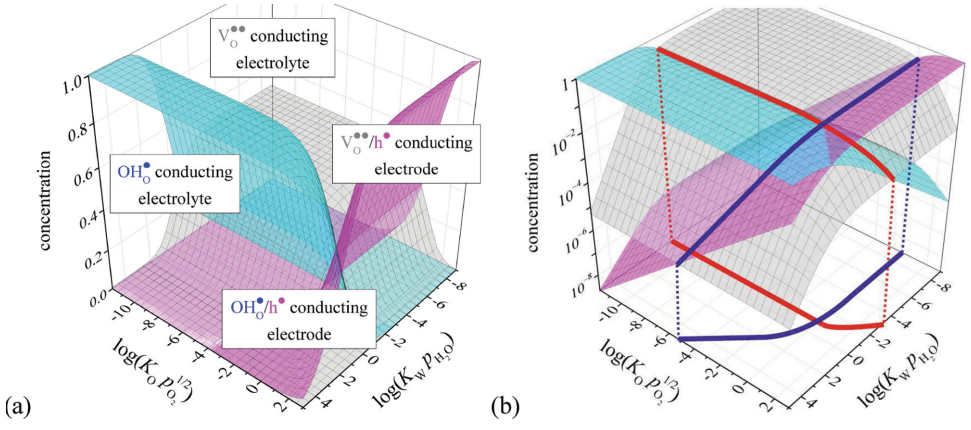

Figure 2. Concentrations (molar fraction) of oxygen vacancies $V_O^{\bullet\bullet}$ (grey), protons $OH_O^{\bullet}$ (blue), and holes $h^{\bullet}$ (pink) in an acceptor-doped oxide ($[A'] = 1$) as functions of $K_O p_{O_2}^{1/2}$ and $K_W p_{H_2O}$. a) linear scale, b) logarithmic concentration scale, the red and blue lines mark the intersections with $[V_O^{\bullet\bullet}] = [OH_O^{\bullet}]$ and $[V_O^{\bullet\bullet}] = [h^{\bullet}]$; also their projections to the base plane are shown.

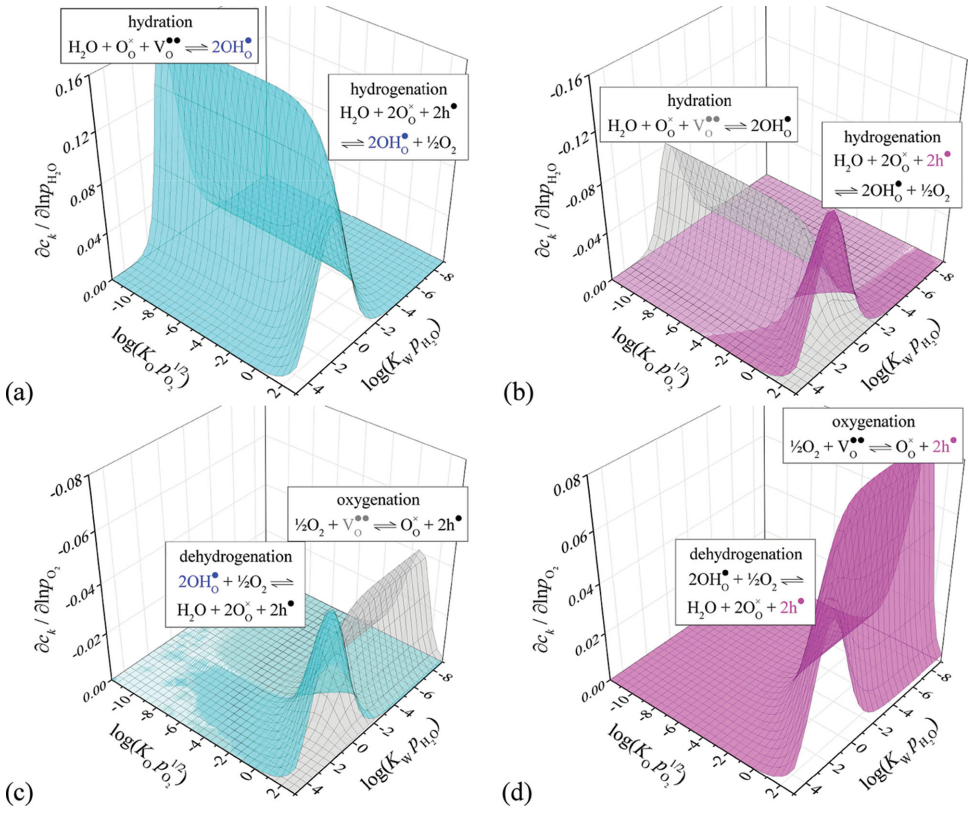

Figure 3. Equilibrium response of bulk defect concentrations ($OH_O^{\bullet}$: light blue, $V_O^{\bullet\bullet}$: grey, $h^{\bullet}$: pink) to changes in p_{H_2O} a,b); and changes in p_{O_2} c,d) calculated from the defect model. The dominating reactions for equilibration with the gas phase in the corresponding regimes are indicated: in b) proton uptake after p_{H_2O} increase occurs either mainly by acid–base reaction in the hind left section or by hydrogenation in the front right part; in c) oxidation after p_{O_2} increase largely occurs by oxygen incorporation (hind right) or by dehydrogenation (front left).

$$C_H^{\delta} \equiv F^2 \frac{\partial c_H}{\partial \mu_H} = 2F^2 \frac{\partial [OH_O^{\bullet}]}{RT\, \partial \ln p_{H_2O}} \tag{5}$$

The sensitivity of other defects to p_{H_2O} and p_{O_2} changes can be expressed by similar partial derivatives $\partial[h^{\bullet}]/\partial \ln p_{O_2}$, $\partial[OH_O^{\bullet}]/\partial \ln p_{O_2}$, $\partial[V_O^{\bullet\bullet}]/\partial \ln p_{H_2O}$, and $\partial[h^{\bullet}]/\partial \ln p_{H_2O}$. **Figure 3** illustrates the response regimes to a p_{H_2O} or p_{O_2} change. For "electrolyte-type" materials with comparably low $[h^{\bullet}]$ but high $[V_O^{\bullet\bullet}]$ and/or $[OH_O^{\bullet}]$ (located in the left regions of the plots in Figure 3) an increased p_{H_2O} leads to predominantly water uptake by acid–base reaction (2): the grey surface in Figure 3b (change of $[V_O^{\bullet\bullet}]$) lies much higher than the pink surface ([h] change).

For materials with high hole conductivity located in the front right part of the plots in Figure 3, an increase of p_{H_2O} can lead to two situations: (i) for materials and conditions characterized by $[V_O^{\bullet\bullet}] > [h^{\bullet}]$, despite a perceptible hole concentration, the thermodynamics is still dominated by the acid–base reaction (2) leading to predominant incorporation of protons and oxide ions (i.e., the grey surface in Figure 3b representing the $[V_O^{\bullet\bullet}]$ change is still higher than the pink surface giving the $[h^{\bullet}]$ changes), (ii) for $[V_O^{\bullet\bullet}] < [h^{\bullet}]$ protons will mainly be incorporated at expense of holes by redox reaction (3). Note that for a given material a sufficiently large change in p_{O_2} switching the ratio of $[V_O^{\bullet\bullet}]$ and $[h^{\bullet}]$ will switch thermodynamics between predominant hydration and predominant proton uptake via redox reaction.[30] An increase of p_{O_2} will lead to increased hole concentration either by predominant oxygen uptake according to reaction (1) (low $[OH_O^{\bullet}]$, right corner), or by formation of holes at the expense of protonic defects by inverse reaction (3) (high $[OH_O^{\bullet}]$, front corner).

Within the model of ideally dilute defects, the boundary between the different regimes – proton uptake by redox or by acid–base reaction as obtained from the partial derivatives in Figure 3b directly corresponds to the intersection of the $[V_O^{\bullet\bullet}]$ and $[h^{\bullet}]$ surfaces (blue line in Figure 2), i.e., the knowledge of $[V_O^{\bullet\bullet}]$ being larger or smaller than $[h^{\bullet}]$ suffices to predict the proton uptake reaction. A similar relation holds for the boundary between oxidation after a p_{O_2} change by either oxygen uptake (for $[V_O^{\bullet\bullet}] > [OH_O^{\bullet}]$) or hydrogen excorporation ($[V_O^{\bullet\bullet}] < [OH_O^{\bullet}]$). Deviations may occur for materials with nondilute defects. These considerations demonstrate that in a system with three carriers already the thermodynamics of the stoichiometry changes exhibits quite a complex behavior.

3. Diffusion Kinetics for Three Mobile Carriers: Analytical Relations

In this section we derive the general flux equations for diffusion in a system with three mobile carriers with different

mobilities, which in the case of perovskites are protons, oxygen vacancies, and holes. Here it is important to note that this set of three defects is characterized by the fact that they are not necessarily in local defect-chemical equilibrium with each other (a system of, e.g., protons, holes, and electrons where the latter are always in equilibrium by the internal band–band reaction with the holes will behave as a two-carrier system). If interactions between the three carriers are neglected (dilute limit) the flux equations can, in the standard way, be expressed as proportionalities to the respective gradients in their electrochemical potentials:[4,11,49]

$$\begin{pmatrix} J_{V_O^{\cdot\cdot}} \\ J_{H_i^{\cdot}} \\ J_{h^{\cdot}} \end{pmatrix} = -\frac{1}{F^2}\begin{pmatrix} \sigma_{V_O^{\cdot\cdot}}/4 & 0 & 0 \\ 0 & \sigma_{H_i^{\cdot}} & 0 \\ 0 & 0 & \sigma_{h^{\cdot}} \end{pmatrix}\begin{pmatrix} \nabla\tilde{\mu}_{V_O^{\cdot\cdot}} \\ \nabla\tilde{\mu}_{H_i^{\cdot}} \\ \nabla\tilde{\mu}_{h^{\cdot}} \end{pmatrix} \quad (6)$$

Here for brevity we designate the protonic defects as interstitial protons $H_i^{\cdot}$ rather than OH^- on O^{2-} sites (i.e., $OH_O^{\cdot}$). Even though the latter is more precise, it is less concise and might incorrectly suggest OH^- transport. When writing $H_i^{\cdot}$ we understand the site i to be associated with the regular O^{2-} (this is pretty formal as the radius of OH^- is even smaller than that of O^{2-}). The transition from defect to component level reads.[33b]

$$\begin{aligned} \nabla\mu_O &= \nabla\tilde{\mu}_{O^{2-}} - 2\nabla\tilde{\mu}_{e^-} = -\nabla\tilde{\mu}_{V_O^{\cdot\cdot}} + 2\nabla\tilde{\mu}_{h^{\cdot}} \\ \nabla\mu_H &= \nabla\tilde{\mu}_{H^+} + \nabla\tilde{\mu}_{e^-} = \nabla\tilde{\mu}_{H_i^{\cdot}} - \nabla\tilde{\mu}_{h^{\cdot}} \end{aligned} \quad (7)$$

Charge conservation implies

$$\sum z_k J_k = (2J_{V_O^{\cdot\cdot}} + J_{H_i^{\cdot}} + J_{h^{\cdot}}) = 0 \quad (8)$$

Using these equations, the electrochemical potential gradient of holes can be expressed in terms of the chemical potential gradients of the components O and H[31–33]

$$\nabla\tilde{\mu}_{h^{\cdot}} = \frac{t_{V_O^{\cdot\cdot}}}{2}\nabla\mu_O - t_{H_i^{\cdot}}\nabla\mu_H \quad (9)$$

with $t_k = \sigma_k/\Sigma_k\sigma_k$ = transference number of carrier k. Thus, oxygen vacancy and proton fluxes can be expressed as

$$\begin{aligned} J_{V_O^{\cdot\cdot}} &= \frac{\sigma_{V_O^{\cdot\cdot}}(1-t_{V_O^{\cdot\cdot}})}{4F^2}\nabla\mu_O + \frac{\sigma_{V_O^{\cdot\cdot}}t_{H_i^{\cdot}}}{2F^2}\nabla\mu_H \\ J_{H_i^{\cdot}} &= -\frac{\sigma_{H_i^{\cdot}}t_{V_O^{\cdot\cdot}}}{2F^2}\nabla\mu_O - \frac{\sigma_{H_i^{\cdot}}(1-t_{H_i^{\cdot}})}{F^2}\nabla\mu_H \end{aligned} \quad (10)$$

Alternatively, $J_{V_O^{\cdot\cdot}}$ and $J_{H^{\cdot}}$ can be written as functions of water and oxygen potential gradients ($\nabla\mu_{H_2O} = \nabla\mu_O + 2\nabla\mu_H$)

$$\begin{aligned} J_{V_O^{\cdot\cdot}} &= \frac{\sigma_{V_O^{\cdot\cdot}}t_{h^{\cdot}}}{4F^2}\nabla\mu_O + \frac{\sigma_{V_O^{\cdot\cdot}}t_{H_i^{\cdot}}}{4F^2}\nabla\mu_{H_2O} \\ J_{H_i^{\cdot}} &= \frac{\sigma_{H_i^{\cdot}}t_{h^{\cdot}}}{2F^2}\nabla\mu_O - \frac{\sigma_{H_i^{\cdot}}(1-t_{H_i^{\cdot}})}{2F^2}\nabla\mu_{H_2O} \end{aligned} \quad (11)$$

Up to this point (and apart from a sign mistake in the first term of Equation (11b) in Kim and Yoo[13] which should be "+" not "–") our treatment is identical to that given in the same study. In the usual treatment of the two carrier case (and tentatively for the three carrier case in the study by Kim and Yoo)[13] $\nabla\mu_O$ (and analogously $\nabla\mu_{H_2O}$ or $\nabla\mu_H$) is written as $(\partial\mu_O/\partial c_O)\nabla c_O$ whereupon $(\partial\mu_O/\partial c_O)$ combined with the prefactor to $\nabla\mu_O$ yields the respective diffusion coefficient. However, in the case of a system with three carriers this is not correct, rather $\nabla\mu_O$ is not a unique function of c_O but also depends on c_H, hence

$$\nabla\mu_O = \frac{\partial\mu_O}{\partial c_O}\nabla c_O + \frac{\partial\mu_O}{\partial c_H}\nabla c_H \quad (12)$$

A precise procedure directly leading to diffusion coefficients is the following: We convert the component potentials into chemical potentials of the defects which for dilute conditions solely depend on the respective defect concentrations ($\mu_k = \mu_k^0 + RT\ln c_k$). Thus,

$$\begin{aligned} \nabla\mu_O &= -\nabla\mu_{V_O^{\cdot\cdot}} + 2\nabla\mu_{h^{\cdot}} \\ \nabla\mu_H &= \nabla\mu_{H_i^{\cdot}} - \nabla\mu_{h^{\cdot}} \end{aligned} \quad (13)$$

where now $\nabla\mu_k = \nabla c_k \cdot \mathrm{d}\mu_k/\mathrm{d}c_k = RT\cdot\nabla c_k/c_k$ (ideally dilute situation for the defects). Using the Nernst–Einstein equation $D_k = RT\sigma_k/(c_k z_k^2 F^2)$ this leads to

$$J_{V_O^{\cdot\cdot}} = -D_{V_O^{\cdot\cdot}}(1-t_{V_O^{\cdot\cdot}})\nabla c_{V_O^{\cdot\cdot}} + \frac{1}{2}D_{H_i^{\cdot}}t_{V_O^{\cdot\cdot}}\nabla c_{H_i^{\cdot}} + \frac{1}{2}D_{h^{\cdot}}t_{V_O^{\cdot\cdot}}\nabla c_{h^{\cdot}} = -J_O \quad (14)$$

$$J_{H_i^{\cdot}} = 2D_{V_O^{\cdot\cdot}}t_{H_i^{\cdot}}\nabla c_{V_O^{\cdot\cdot}} - D_{H_i^{\cdot}}(1-t_{H_i^{\cdot}})\nabla c_{H_i^{\cdot}} + D_{h^{\cdot}}t_{H_i^{\cdot}}\nabla c_{h^{\cdot}} = J_H \quad (15)$$

with defect diffusivities D_k (cf. also Yu et al.)[18] Note the similarity of Equations (14) and (15) to the two carrier situation, e.g., for the ambipolar motion of vacancies and holes constituting chemical diffusion of oxygen in a proton-free oxide, described by

$$J_{V_O^{\cdot\cdot}} = -D_{V_O^{\cdot\cdot}}(1-t_{V_O^{\cdot\cdot}})\nabla c_{V_O^{\cdot\cdot}} + \frac{1}{2}D_{h^{\cdot}}t_{V_O^{\cdot\cdot}}\nabla c_{h^{\cdot}} \quad (16)$$

There, however, because of $2\nabla c_{V_O^{\cdot\cdot}} = -\nabla c_{h^{\cdot}}$ a single diffusion coefficient D_O^{δ} results, given by the well-known relation $D_O^{\delta} = (1-t_{V_O^{\cdot\cdot}})D_{V_O^{\cdot\cdot}} + t_{V_O^{\cdot\cdot}}D_{h^{\cdot}}$.[7,34] Another example is the ambipolar motion of oxygen vacancies and excess protons in an exclusively ion-conducting perovskite. Here the vacancy flux is given by

$$J_{V_O^{\cdot\cdot}} = -D_{V_O^{\cdot\cdot}}(1-t_{V_O^{\cdot\cdot}})\nabla c_{V_O^{\cdot\cdot}} + \frac{1}{2}D_{H_i^{\cdot}}t_{V_O^{\cdot\cdot}}\nabla c_{H_i^{\cdot}} \quad (17)$$

and owing to electroneutrality the single $D_{H_2O}^{\delta}$ is specified by $D_{H_2O}^{\delta} = (1-t_{V_O^{\cdot\cdot}})D_{V_O^{\cdot\cdot}} + t_{V_O^{\cdot\cdot}}D_{OH_O^{\cdot}}$. For systems with three carriers, besides $\nabla c_{V_O^{\cdot\cdot}}$ Equation (14) contains contributions from $\nabla c_{h^{\cdot}}$ as well as $\nabla c_{H_i^{\cdot}}$ because both protons and holes together supply charge compensation. Local electroneutrality allows us to eliminate one gradient out of three, but we are still left with $J_{V_O^{\cdot\cdot}}$ depending on two gradients which are not simply proportional to each other.

In the following we concentrate on the representation in terms of $\nabla c_{V_O^{\cdot\cdot}}$ and $\nabla c_{H_i^{\cdot}}$, and the relations for $J_{V_O^{\cdot\cdot}}$, $J_{OH_O^{\cdot}}$, and $J_{h^{\cdot}}$ (which is redundant, cf. Equation (8)) are given. The terms

in square brackets correspond to the respective diffusion coefficients which can be traced back to defect diffusivities $D_{V_O^{\cdot\cdot}}, D_{H_i^{\cdot}}, D_{h^{\cdot}}$ and defect concentrations contained in the transference numbers

$$J_{V_O^{\cdot\cdot}} = -\left[(1-t_{V_O^{\cdot\cdot}})D_{V_O^{\cdot\cdot}} + t_{V_O^{\cdot\cdot}}D_{h^{\cdot}}\right]\nabla c_{V_O^{\cdot\cdot}} - \frac{1}{2}\left[t_{V_O^{\cdot\cdot}}(D_{h^{\cdot}} - D_{H_i^{\cdot}})\right]\nabla c_{H_i^{\cdot}} \quad (18)$$

$$J_{H_i^{\cdot}} = -2\left[t_{H_i^{\cdot}}(D_{h^{\cdot}} - D_{V_O^{\cdot\cdot}})\right]\nabla c_{V_O^{\cdot\cdot}} - \left[(1-t_{H_i^{\cdot}})D_{H_i^{\cdot}} + t_{H_i^{\cdot}}D_{h^{\cdot}}\right]\nabla c_{H_i^{\cdot}} \quad (19)$$

$$J_{h^{\cdot}} = -(-2)\left[t_{h^{\cdot}}D_{V_O^{\cdot\cdot}} + (1-t_{h^{\cdot}})D_{h^{\cdot}}\right]\nabla c_{V_O^{\cdot\cdot}} - (-1)\left[t_{h^{\cdot}}D_{H_i^{\cdot}} + (1-t_{h^{\cdot}})D_{h^{\cdot}}\right]\nabla c_{H_i^{\cdot}} \quad (20)$$

This can conveniently be expressed in matrix form where in the diffusion coefficient $D^k_{l(m)}$ the superscript denotes the species whose flux is considered. The subscripts refer to concentration gradients, the first to the directly driving gradient and the second (in brackets) to the other gradient

$$\begin{pmatrix} J_{V_O^{\cdot\cdot}} \\ J_{H_i^{\cdot}} \\ J_{h^{\cdot}} \end{pmatrix} \equiv -\begin{pmatrix} D^{V}_{V(H)} & 1/2\,D^{V}_{H(V)} \\ 2D^{H}_{V(H)} & D^{H}_{H(V)} \\ -2D^{h}_{V(H)} & -D^{h}_{H(V)} \end{pmatrix}\begin{pmatrix} \nabla c_{V_O^{\cdot\cdot}} \\ \nabla c_{H_i^{\cdot}} \end{pmatrix} \quad (21)$$

There are more rows than columns in the matrix because one of the flux equations is redundant. In other words: four effective diffusion coefficients (constituting two rows) suffice to describe the system. **Table 1** shows the interrelations between them indicating that even an arbitrary selection of four effective diffusivities suffices. It is important to note that different types of diffusion coefficients appear:

i. Direct terms $D^k_{k(m)}$ for the contribution to J_k driven by ∇c_k, e.g., $D^{V}_{V(H)} \equiv (1-t_{V_O^{\cdot\cdot}})D_{V_O^{\cdot\cdot}} + t_{V_O^{\cdot\cdot}}D_{h^{\cdot}}$ (more specifically, for a situation with $\nabla c_k \neq 0$ but $\nabla c_m = 0$, $D^k_{k(m)}$ determines the flux $J_k = -D^k_{k(m)}\nabla c_k$ of defect k). These direct terms are always positive. They are isomorphic to diffusivities in two-carrier problems (e.g., $D^{\delta}_{O^{\cdot\cdot}} = (1-t_{V_O^{\cdot\cdot}})D_{V_O^{\cdot\cdot}} + t_{V_O^{\cdot\cdot}}D_{h^{\cdot}}$) but not identical to them as now the transference numbers contain contributions from a third carrier ($1-t_{V_O^{\cdot\cdot}} = t_{h^{\cdot}} + t_{H_i^{\cdot}}$).
ii. Indirect terms $D^k_{l(k)}$ such as $D^{V}_{H(V)} \equiv t_{V_O^{\cdot\cdot}}(D_{h^{\cdot}} - D_{H_i^{\cdot}})$, which describes the diffusion coefficient for $V_O^{\cdot\cdot}$ if $\nabla c_{V_O^{\cdot\cdot}} = 0$ but $\nabla c_{H_i^{\cdot}}$ is the driving force. They may have positive or negative signs depending on the actual defect diffusivities. It is important to note that the presence of a second concentration gradient in the flux equations opens the possibility for uphill diffusion of a species as regards its own concentration gradient as driver. It is not mandatory that indirect terms such as $D^{V}_{H(V)}$ become negative, the uphill flux can also be caused by the corresponding concentration gradient having the opposite sign to the gradient related to the direct diffusion coefficient (as it is the case in the numerical examples given in Section 4). Of course all processes are still downhill in terms of electrochemical potential gradients. Note that Onsager's symmetry principle does not apply to the terms in Equation (21).[35] It holds for the representation of J in terms of transport matrix L and gradient in electrochemical potential $\nabla\tilde{\mu}$ (cf. Equation (6), yet in our case the cross terms are set to zero corresponding to the absence of defect interactions).

Table 1. Diffusion coefficients from Equations (21)–(32) expressed in terms of defect diffusivities D_k and transference numbers t_k. Additionally, all diffusion coefficients $D^k_{l(m)}$ are traced back to $D^{V}_{V(H)}$, $D^{H}_{H(V)}$, $D^{V}_{H(V)}$, $D^{H}_{V(H)}$ (however, which set of four diffusion coefficients is chosen to express the other terms is arbitrary). For situations characterized by $D_{h^{\cdot}}$ $D_{H_i^{\cdot}}$ $D_{V_O^{\cdot\cdot}}$, the $D^k_{l(k)}$ indirect terms are positive.

$D^k_{l(m)}$	$D^k_{l(m)}(t_k, D_k, D_l, D_m)$	Interrelations,	...to $D^{V}_{V(H)}$, $D^{H}_{H(V)}$, $D^{V}_{H(V)}$, $D^{H}_{V(H)}$
$D^{V}_{V(H)}$	$(1-t_{V_O^{\cdot\cdot}})D_{V_O^{\cdot\cdot}} + t_{V_O^{\cdot\cdot}}D_{h^{\cdot}}$	$= D^{V}_{h(H)}$	
$D^{h}_{V(H)}$	$t_{h^{\cdot}}D_{V_O^{\cdot\cdot}} + (1-t_{h^{\cdot}})D_{h^{\cdot}}$	$= D^{h}_{h(H)}$	$= D^{V}_{V(H)} + D^{H}_{V(H)}$
$D^{H}_{H(V)}$	$(1-t_{H_i^{\cdot}})D_{H_i^{\cdot}} + t_{H_i^{\cdot}}D_{h^{\cdot}}$	$= D^{H}_{h(V)}$	
$D^{h}_{H(V)}$	$t_{h^{\cdot}}D_{H_i^{\cdot}} + (1-t_{h^{\cdot}})D_{h^{\cdot}}$	$= D^{h}_{h(V)}$	$= D^{H}_{H(V)} + D^{V}_{H(V)}$
$D^{V}_{V(h)}$	$(1-t_{V_O^{\cdot\cdot}})D_{V_O^{\cdot\cdot}} + t_{V_O^{\cdot\cdot}}D_{H_i^{\cdot}}$	$= D^{V}_{H(h)}$	$= D^{V}_{V(H)} - D^{V}_{H(V)}$
$D^{H}_{V(h)}$	$(1-t_{H_i^{\cdot}})D_{H_i^{\cdot}} + t_{H_i^{\cdot}}D_{V_O^{\cdot\cdot}}$	$= D^{H}_{H(h)}$	$= D^{H}_{H(V)} - D^{V}_{V(H)} - D^{H}_{V(H)}$
$D^{V}_{H(V)}$	$t_{V_O^{\cdot\cdot}}(D_{h^{\cdot}} - D_{H_i^{\cdot}})$	$= D^{V}_{h(V)}$	
$D^{H}_{V(H)}$	$t_{H_i^{\cdot}}(D_{h^{\cdot}} - D_{V_O^{\cdot\cdot}})$	$= D^{H}_{h(H)}$	
$D^{h}_{V(h)}$	$t_{h^{\cdot}}(D_{H_i^{\cdot}} - D_{V_O^{\cdot\cdot}})$	$= D^{h}_{H(h)}$	$= D^{H}_{H(V)} - D^{V}_{V(H)} + D^{V}_{H(V)} - D^{H}_{V(H)}$

The fact that the indirect terms $D^{k}_{l(k)}$ show up in Equations (18), (19), and (21), where the flux is expressed in terms of charged defects, emphasizes that they appear through the electrical potential gradient. In the present case $D_{h^\bullet} - D_{H_i^\bullet}$ and $D_{h^\bullet} - D_{V_O^{\bullet\bullet}}$ are positive. The nonmonotonicity in hole concentration upon p_{H_2O} change (Figures 6 and 7) shows that this does not require the indirect terms to be negative.

iii. Finally, there are terms denoted by $D^{k}_{l(m)}$ where all three indices k,l,m differ from each other, such as $D^{h}_{H(V)} \equiv t_{h^\bullet} D_{H_i^\bullet} + (1-t_{h^\bullet}) D_{h^\bullet}$ in $J_{h^\bullet}$. They correspond to the diffusion coefficient of defect k when ∇c_l is taken as driving force and ∇c_m disappears. They exhibit the same isomorphicity to chemical diffusivities of the two-carrier case and are positive, but they appear with a negative sign in Equations (20) and (21). This is caused by the fact that they describe the flux of species k driven by the other two concentration gradients l and m, i.e., coupled by the electroneutrality condition leading to a counter flow of defects with identical sign. Generally, these terms can be written in the form of $\frac{\sigma_{h^\bullet} + \sigma_{H_i^\bullet}}{\sigma_{tot}} D_{V_O^{\bullet\bullet}} + \frac{\sigma_{V_O^{\bullet\bullet}}}{\sigma_{tot}} D_{h^\bullet}$ and $\frac{\sigma_{h^\bullet}}{\sigma_{tot}} D_{V_O^{\bullet\bullet}} + \frac{\sigma_{V_O^{\bullet\bullet}} + \sigma_{H_i^\bullet}}{\sigma_{tot}} D_{h^\bullet}$. However, in contrast to the two-carrier system now $t_{h^\bullet} + t_{H_i^\bullet} = 1 - t_{V_O^{\bullet\bullet}} \neq t_{h^\bullet}$ and therefore $D^{h}_{H(V)} \neq D^{V}_{H(V)}$. Note that the relations $D^{h}_{V(H)} = D^{V}_{V(H)} + 2t_{H_i^\bullet}(D_{h^\bullet} - D_{V_O^{\bullet\bullet}})$ and $D^{h}_{H(V)} = D^{V}_{H(V)} + \frac{1}{2} t_{V_O^{\bullet\bullet}}(D_{h^\bullet} - D_{H_i^\bullet})$ hold, i.e., all defect fluxes can be expressed by four diffusivity terms (Table 1). The difference $D^{h}_{V(H)} - D^{V}_{V(H)}$ yields $D^{V}_{H(V)} \equiv t_{V_O^{\bullet\bullet}}(D_{h^\bullet} - D_{H_i^\bullet})$ which is the diffusion coefficient describing vacancy flux under a proton gradient if $\nabla c_{V_O^{\bullet\bullet}} = 0$ ($\nabla c_{h^\bullet} \neq 0$ and $\nabla c_{H_i^\bullet} \neq 0$ in Equation (19)).

Let us exemplify the meaning of Equations (18)–(20) for a hypothetical situation where $\nabla c_{V_O^{\bullet\bullet}} = 0$ (note that this condition will hold only for an instantaneous snapshot since in the further evolution $\nabla c_{V_O^{\bullet\bullet}} \neq 0$ may build up, even if $[V_O^{\bullet\bullet}]_{t=0} = [V_O^{\bullet\bullet}]_{final}$). Then

$$J_{V_O^{\bullet\bullet}} = -\left[1/2t_{V_O^{\bullet\bullet}}(D_{h^\bullet} - D_{H_i^\bullet})\right]\nabla c_{H_i^\bullet} = -1/2 D^{V}_{H(V)} \nabla c_{H_i^\bullet} \quad (22)$$

$$J_{H_i^\bullet} = -\left[(1-t_{H_i^\bullet})D_{H_i^\bullet} + t_{H_i^\bullet} D_{h^\bullet}\right]\nabla c_{H_i^\bullet} = -D^{H}_{H(V)} \nabla c_{H_i^\bullet} \quad (23)$$

$$J_{h^\bullet} = -\left[-t_{h^\bullet} D_{H_i^\bullet} - (1-t_{h^\bullet})D_{h^\bullet})\right]\nabla c_{H_i^\bullet} = -(-D^{h}_{H(V)} \nabla c_{H_i^\bullet}) \quad (24)$$

This means that although $\nabla c_{V_O^{\bullet\bullet}} = 0$ the $V_O^{\bullet\bullet}$ flux does in general not vanish (it would vanish only for $D_{h^\bullet} = D_{H_i^\bullet}$; or for $t_{V_O^{\bullet\bullet}} = 0$, i.e., the proton/hole two carrier case). Rather, the nonzero $J_{V_O^{\bullet\bullet}}$ is the result of the fact that for different proton and hole diffusivities their fluxes, Equations (23) and (24)—despite having opposite directions—do not exactly cancel because of $(1-t_{H_i^\bullet}) \neq t_{h^\bullet}$. Thus, a $V_O^{\bullet\bullet}$ flux as described by the indirect terms in Equations (18) and (22) is required to maintain electroneutrality. Depending on the relative magnitudes of $D_{h^\bullet}, D_{H_i^\bullet}$, the direction of $J_{V_O^{\bullet\bullet}}$ may change. This situation is depicted in **Figure 4**. In the presently considered general

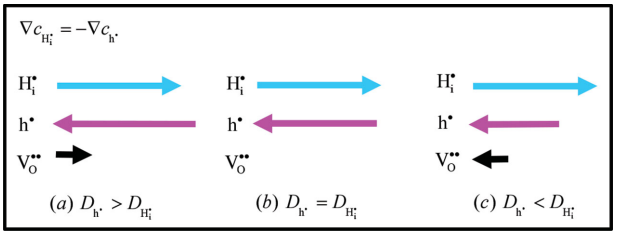

Figure 4. Schematic defect fluxes for $\nabla c_{H_i^\bullet} = -\nabla c_{h^\bullet}$ and a situation with perceptible $V_O^{\bullet\bullet}$ concentration and mobility (i.e., $t_{V_O^{\bullet\bullet}} > 0$) but $\nabla c_{V_O^{\bullet\bullet}} = 0$: a) $D_{h^\bullet} > D_{H_i^\bullet}$, b) $D_{h^\bullet} = D_{H_i^\bullet}$, c) $D_{h^\bullet} < D_{H_i^\bullet}$. The length of the arrows represents the current $z_k J_k$. The direction of $J_{V_O^{\bullet\bullet}}$ is determined by the indirect term in Equation (18) and changes depending on $D_{h^\bullet}$ being larger or smaller than $D_{H_i^\bullet}$.

case protons as interstitial defects, oxygen vacancies and holes as electronic defects do not interact, but are coupled via electroneutrality. Site balance is not really an issue owing to the conditions (even in a real perovskite mixed conductor with protons being attached to oxide ions and holes possibly being localized at oxide ions this is a reasonable approximation since even the highest observed $[V_O^{\bullet\bullet}] \approx 0.5$ are low compared to the three oxygen sites per formula unit and $V_O^{\bullet\bullet}$ formation will not restrict formation of $OH_O^\bullet$ and $h^\bullet$ via site exhaustion; indirect mutual influence such as hole concentration affecting proton uptake via decreasing the basicity of regular oxide ions may lead to activity coefficients deviating from one). Thus the defect concentrations and their changes are exclusively coupled by the electroneutrality condition. However one can imagine different situations where defects are strongly coupled to each other additionally by site balance, which could then also lead to cross terms.

Alternatively, the defect fluxes may also be expressed by any other pair of defect gradients; the equations are redundant but given here for completeness

$$\begin{aligned} J_{V_O^{\bullet\bullet}} = &-\left[(1-t_{V_O^{\bullet\bullet}})D_{V_O^{\bullet\bullet}} + t_{V_O^{\bullet\bullet}} D_{H_i^\bullet}\right]\nabla c_{V_O^{\bullet\bullet}} \\ &-(-1/2)\left[t_{V_O^{\bullet\bullet}}(D_{h^\bullet} - D_{H_i^\bullet})\right]\nabla c_{h^\bullet} \end{aligned} \quad (25)$$

$$\begin{aligned} J_{H_i^\bullet} = &-(-2)\left[(1-t_{H_i^\bullet})D_{H_i^\bullet} + t_{H_i^\bullet} D_{V_O^{\bullet\bullet}}\right]\nabla c_{V_O^{\bullet\bullet}} \\ &-(-1)\left[(1-t_{H_i^\bullet})D_{H_i^\bullet} + t_{H_i^\bullet} D_{h^\bullet}\right]\nabla c_{h^\bullet} \end{aligned} \quad (26)$$

$$\begin{aligned} J_{h^\bullet} = &-2\left[t_{h^\bullet}(D_{H_i^\bullet} - D_{V_O^{\bullet\bullet}})\right]\nabla c_{V_O^{\bullet\bullet}} \\ &-\left[t_{h^\bullet} D_{H_i^\bullet} + (1-t_{h^\bullet})D_{h^\bullet})\right]\nabla c_{h^\bullet} \end{aligned} \quad (27)$$

$$\begin{pmatrix} J_{V_O^{\bullet\bullet}} \\ J_{H_i^\bullet} \\ J_{h^\bullet} \end{pmatrix} \equiv - \begin{pmatrix} D^{V}_{V(h)} & -1/2 D^{V}_{h(V)} \\ -2D^{H}_{V(h)} & -D^{H}_{h(V)} \\ 2D^{h}_{V(h)} & D^{h}_{h(V)} \end{pmatrix} \begin{pmatrix} \nabla c_{V_O^{\bullet\bullet}} \\ \nabla c_{h^\bullet} \end{pmatrix} \quad (28)$$

$$\begin{aligned} J_{V_O^{\bullet\bullet}} = &-(-1/2)\left[(1-t_{V_O^{\bullet\bullet}})D_{V_O^{\bullet\bullet}} + t_{V_O^{\bullet\bullet}} D_{H_i^\bullet}\right]\nabla c_{H_i^\bullet} \\ &-(-1/2)\left[(1-t_{V_O^{\bullet\bullet}})D_{V_O^{\bullet\bullet}} + t_{V_O^{\bullet\bullet}} D_{h^\bullet}\right]\nabla c_{h^\bullet} \end{aligned} \quad (29)$$

$$J_{\mathrm{H_i^{\cdot}}} = -\left[(1-t_{\mathrm{H_i^{\cdot}}})D_{\mathrm{H_i^{\cdot}}} + t_{\mathrm{H_i^{\cdot}}}D_{\mathrm{V_O^{\cdot\cdot}}}\right]\nabla c_{\mathrm{H_i^{\cdot}}} - (-1)\left[t_{\mathrm{H_i^{\cdot}}}(D_{\mathrm{h^{\cdot}}} - D_{\mathrm{V_O^{\cdot\cdot}}})\right]\nabla c_{\mathrm{h^{\cdot}}} \quad (30)$$

$$J_{\mathrm{h^{\cdot}}} = -(-1)\left[t_{\mathrm{h^{\cdot}}}(D_{\mathrm{H_i^{\cdot}}} - D_{\mathrm{V_O^{\cdot\cdot}}})\right]\nabla c_{\mathrm{H_i^{\cdot}}} - \left[t_{\mathrm{h^{\cdot}}}D_{\mathrm{V_O^{\cdot\cdot}}} + (1-t_{\mathrm{h^{\cdot}}})D_{\mathrm{h^{\cdot}}}\right]\nabla c_{\mathrm{h^{\cdot}}} \quad (31)$$

$$\begin{pmatrix} J_{\mathrm{V_O^{\cdot\cdot}}} \\ J_{\mathrm{H_i^{\cdot}}} \\ J_{\mathrm{h^{\cdot}}} \end{pmatrix} \equiv -\begin{pmatrix} -1/2D^{\mathrm{V}}_{\mathrm{H(h)}} & -1/2D^{\mathrm{V}}_{\mathrm{h(H)}} \\ D^{\mathrm{H}}_{\mathrm{H(h)}} & -D^{\mathrm{H}}_{\mathrm{h(H)}} \\ -D^{\mathrm{h}}_{\mathrm{H(h)}} & D^{\mathrm{h}}_{\mathrm{h(H)}} \end{pmatrix}\begin{pmatrix} \nabla c_{\mathrm{H_i^{\cdot}}} \\ \nabla c_{\mathrm{h^{\cdot}}} \end{pmatrix} \quad (32)$$

In total, in Equations (18)–(32), 18 individual diffusivity terms appear, many of which are identical. The remaining nine diffusion coefficients can all be traced back to the set of four diffusivities from Equation (21) as indicated in Table 1. For the well-known situations where the flux of one carrier is negligible Equations (18)–(32) converge properly towards the well-established single chemical diffusion coefficient. For water incorporation into an electrolyte with negligible hole flux (negligible hole concentration and/or mobility) $\nabla c_{\mathrm{h^{\cdot}}} = 0$ holds, corresponding to $\nabla c_{\mathrm{V_O^{\cdot\cdot}}} = -\frac{1}{2}\nabla c_{\mathrm{H_i^{\cdot}}} = -\nabla c_{\mathrm{H_2O}}$, and thus Equation (18) transforms into the well-known equation for chemical diffusion of water $-J_{\mathrm{H_2O}} = J_{\mathrm{V_O^{\cdot\cdot}}} = -\left[t_{\mathrm{H_i^{\cdot}}}D_{\mathrm{V_O^{\cdot\cdot}}} + t_{\mathrm{V_O^{\cdot\cdot}}}D_{\mathrm{H_i^{\cdot}}}\right]\nabla c_{\mathrm{V_O^{\cdot\cdot}}} = D^{\delta}_{\mathrm{H_2O}}\nabla c_{\mathrm{H_2O}}$. Also for the case of pure redox reaction (only chemical incorporation of H ($\nabla c_{\mathrm{V_O^{\cdot\cdot}}} = 0, t_{\mathrm{V_O^{\cdot\cdot}}} \approx 0$) or O ($\nabla c_{\mathrm{H_i^{\cdot}}} = 0, t_{\mathrm{H_i^{\cdot}}} \approx 0$) into mixed vacancy/hole or proton/hole conductors), simple single-fold chemical diffusion results from Equations (18) and (20): $J_{\mathrm{V_O^{\cdot\cdot}}} = -\left[t_{\mathrm{h^{\cdot}}}D_{\mathrm{V_O^{\cdot\cdot}}} + t_{\mathrm{V_O^{\cdot\cdot}}}D_{\mathrm{h^{\cdot}}}\right]\nabla c_{\mathrm{V_O^{\cdot\cdot}}} = -D^{\delta}_{\mathrm{O}}\nabla c_{\mathrm{V_O^{\cdot\cdot}}}$ and $J_{\mathrm{H_i^{\cdot}}} = -\left[t_{\mathrm{h^{\cdot}}}D_{\mathrm{H_i^{\cdot}}} + t_{\mathrm{H_i^{\cdot}}}D_{\mathrm{h^{\cdot}}}\right]\nabla c_{\mathrm{H_i^{\cdot}}} = -D^{\delta}_{\mathrm{H}}\nabla c_{\mathrm{H_i^{\cdot}}}$.

The necessity of four distinct diffusivities for quantitative description of the system indicates that the simplistic approach of independent H and O diffusion (i.e., based on only two diffusivities, approximation of independent diffusion into homogeneous medium) cannot reproduce all details of the real system. This was already recognized in the literature.[12] leading to the introduction of a "moving boundary." Because the flux of one defect as given by Equations (18)–(32) always depends on the concentration gradients of two defects which are not connected by a simple relation (∇c_k not directly proportional to $\nabla c_l, \nabla c_m$ and all gradients evolving in time and space), it is obvious that the fluxes of the different defects are related to each other in a complex way. These effects will be illustrated by numerical simulations in Section 4. We notice that even in the interaction-free case (absence of trapping) the situation becomes very colorful. Interactions can be introduced formally via cross coefficients[4,36,37] or simpler via associates.[7]

As a result of the two-component diffusion kinetics as described by Equations (18)–(20), usually a twofold kinetics after the activity change of one component is expected for a system with three carriers. Only in specific situations the simpler case of onefold relaxation occurs:

i. The transference number of one of the carriers vanishes. Then this carrier acts as an immobile dopant, and the system contains only two mobile carriers.
ii. The defect diffusivities of all three defects are identical (which, if it occurs at all, would hold only for one particular temperature since in general the activation energies of defect diffusivities will differ). Note that in general it does not suffice that two defect diffusivities are equal; e.g., setting $D_{\mathrm{h^{\cdot}}} = D_{\mathrm{H_i^{\cdot}}}$ still leaves $J_{\mathrm{H_i^{\cdot}}}$ depending on both $\left[t_{\mathrm{H_i^{\cdot}}}(D_{\mathrm{h^{\cdot}}} - D_{\mathrm{V_O^{\cdot\cdot}}})\right]\nabla c_{\mathrm{V_O^{\cdot\cdot}}}$ and $\left[(1-t_{\mathrm{H_i^{\cdot}}})D_{\mathrm{H_i^{\cdot}}} + t_{\mathrm{H_i^{\cdot}}}D_{\mathrm{h^{\cdot}}}\right]\nabla c_{\mathrm{H_i^{\cdot}}}$ in Equation (19), and a twofold region is predicted (cf. Figure A2b,c in Appendix 2).

It is also worth addressing the question whether we deal with singlefold or twofold kinetics from a thermodynamic point of view. It goes without saying that twofold kinetics is met if thermodynamics (comparison between final and initial state) demands a combination of acid–base and redox reaction (not only change in H_2O content but in addition also in H or O content). But even if we meet an approximately pure acid–base reaction (H_2O uptake), twofold kinetics occurs if the third carrier ($\mathrm{h^{\cdot}}$) has sufficient mobility and concentration. Then the system takes the fastest initial kinetic path for hydrogen, i.e., makes use of hole transport resulting in large transient effects, although in the final state the hole concentration has to approach the initial value again. However, once having followed that path for hydrogen, the overall relaxation (including oxygen uptake) might be even slower compared to the onefold situation (compare Figure 7b to Figure 7a). The fact that not the fastest option wins is also a peculiar consequence of the three carrier complexity.

The possible kinetic regimes can be recognized when the initial $\mathrm{OH_O^{\cdot}}$ and $\mathrm{V_O^{\cdot\cdot}}$ fluxes ($t = 0$, $x = 0$) after a stepwise change of gas composition (corresponding to $\Delta\mu_{\mathrm{H_2O}}$ or $\Delta\mu_{\mathrm{O}}$) are calculated from Equation (11). For this very initial situation, the respective other chemical potential gradient can be set to zero if the other partial pressure is not changed in the gas phase, as the defect concentrations in the sample are still at their initial values (i.e., homogeneously distributed). The results are shown in **Figure 5**, in which the three-dimensional surfaces indicate the initial fluxes $J(t = 0, x = 0)$ of the three defects. For a $p_{\mathrm{H_2O}}$ increase in Figure 5a, the initial flux of protons (light blue mesh) is compensated either mainly by oxygen vacancies (grey surface) close to the left hind edge, or by holes (pink surface) in the middle and right part of the plot. The former corresponds to an initial water flux, the latter to an initial hydrogen flux. Now we can compare these kinetically derived initial component fluxes $J(t = 0, x = 0)$ with the overall stoichiometry change expected after the $p_{\mathrm{H_2O}}$ increase, which was calculated in Section 2. The solid blue line in the base plane marks the boundary between overall acid–base water uptake and hydrogen uptake (cf. Figure 3b). Close to the right front edge, the fluxes predicted by kinetic arguments (initial flux of hydrogen) and equilibrium thermodynamics (overall hydrogen uptake by reaction (3) are consistent with each other, thus singlefold H-uptake occurs (note that this region is characterized by $t_{\mathrm{V_O^{\cdot\cdot}}} \approx 0$ owing to the low $[\mathrm{V_O^{\cdot\cdot}}]$, cf. Figure 2b). A similar situation is found close to the left hind edge: again kinetics (initial water flux) and thermodynamics (overall water uptake by reaction (2)) correspond to each other, leading to singlefold water uptake (note that in this region $t_{\mathrm{h^{\cdot}}} \approx 0$ holds).

However, there is a zone in between where according to the kinetic consideration $J(t = 0, x = 0)$ has changed to initial hydrogen

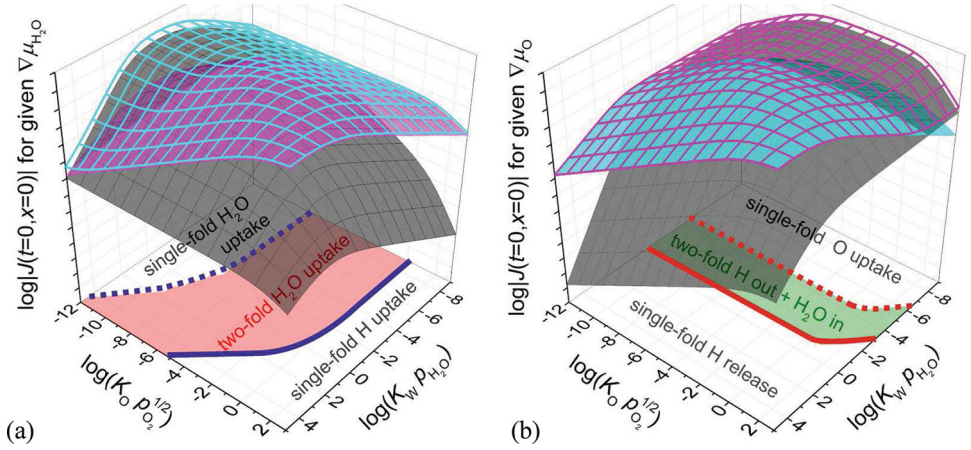

Figure 5. Initial fluxes $J(t = 0, x = 0)$ of $OH_O^{\bullet}$ (light blue surface or mesh), $V_O^{\bullet\bullet}$ (grey surface), and $h^{\bullet}$ (pink surface or mesh); absolute values, in arbitrary units. a) after p_{H_2O} increase, b) after p_{O_2} increase, calculated from Equation (11) with $D_{V_O^{\bullet\bullet}} = 10^{-5}$ cm^2 s^{-1}, $D_{OH_O^{\bullet}} = 10^{-3}$ cm^2 s^{-1}, $D_{h^{\bullet}} = 10^{-1}$ cm^2 s^{-1}. The dotted lines are a projection of the intersection of the $J_{V_O^{\bullet\bullet}}$ and $J_{h^{\bullet}}$ surfaces a) and $J_{V_O^{\bullet\bullet}}$ and $J_{OH_O^{\bullet}}$ surfaces b) into the base plane. When the sum of the two highest fluxes does not add up to a flux of the neutral component (H, O, or H_2O) which according to the thermodynamic regime should be taken up (the solid lines, copied from Figure 3, represent the boundary between water and H uptake in a), and between O uptake and H release in b)), twofold relaxation kinetics is expected—the respective regions are marked red and green in the *xy*-plane. However, the transition between the regimes occurs gradually.

flux (being right of the dashed blue line in Figure 4a) even though equilibrium thermodynamics still predicts essentially a variation of the water content only (being left of the solid blue line). As a consequence, in addition to the initial fast hydrogen uptake, a second (slower) stage with predominant oxygen uptake is needed to achieve the required overall stoichiometry change. This corresponds exactly to the twofold relaxation process with increased complexity compared to the onefold process (with H uptake being faster but O incorporation being slower than chemical diffusion of water, see numerical examples in Section 4).

Similar arguments hold for a p_{O_2} increase, which is shown in Figure 5b. Here, the regions with singlefold relaxation correspond to O uptake (close to hind right edge, region with $t_{OH_O^{\bullet}} \approx 0$) and H excorporation (front left edge, $t_{V_O^{\bullet\bullet}} \approx 0$). In between a zone of twofold oxidation is found where an initial fast outward flux of hydrogen is followed by a second slower stage of water uptake. It would be highly interesting to deliberately look for this—at first glance quite surprising—effect in the relaxation behavior on p_{O_2} changes.

While one of the boundaries between the different kinetic regimes in Figure 5a,b is given by equilibrium defect thermodynamics (the solid blue or red line), the other (the dashed line) depends on the ratios of defect mobilities (cf. Appendix 2). Figure 5 provides a qualitative "map" of onefold and twofold regimes (based only on defect concentrations and mobilities) but cannot yield a full quantitative description. With elapsed time the fluxes deviate from the initial values calculated from Equation (11) because gradients in $\nabla\mu_{H_2O}$ as well as $\nabla\mu_O$ develop in the sample. In particular, the initial fluxes cannot describe the later stage of twofold relaxation (see, e.g., the decrease in effective H diffusivity in **Figure 6**b). Also, the transition between the regimes is not as abrupt as it may seem in Figure 5 but occurs gradually, which is illustrated by the numerical examples in Section 4.

Specifically for the case of water uptake, in ref.[13] a set of two diffusion coefficients ($\tilde{D}_{iH}$ for H uptake, $\tilde{D}_{vH}$ for O) was identified from Equation (11) to describe H and O uptake after a change in p_{H_2O} which depend on defect concentrations and mobilities (in σ_k, t_k) as well as thermodynamic factors $(\partial\mu_{H_2O}/\partial c_{V_O^{\bullet\bullet}}|_{\nabla\mu_O=0}$, $\partial\mu_{H_2O}/\partial c_{OH_O^{\bullet}}|_{\nabla\mu_O=0}$ which can be calculated from the material's defect model. However, it is not unproblematic to use these definitions for calculating the actual fluxes in a sample after p_{H_2O} change according to $J_{H_i^{\bullet}} = -\tilde{D}_{iH}\nabla c_{H_i^{\bullet}}$, $J_{V_O^{\bullet\bullet}} = -\tilde{D}_{vH}\nabla c_{V_O^{\bullet\bullet}}$ because the boundary condition $\nabla\mu_O = 0$ in the partial derivatives is typically violated within the sample In the twofold regime a p_{H_2O} change leads to transient $[h^{\bullet}]$ gradients and thus even if $[V_O^{\bullet\bullet}]$ can approximately be regarded as constant for short times, $\mu_O = -\mu_{V_O^{\bullet\bullet}} + 2\mu_{h^{\bullet}}$ is not constant within the material although p_{O_2} is kept constant (note that this statement does not contradict the use of the conditions $\nabla\mu_{H_2O} = 0$ or $\nabla\mu_O = 0$ for calculation of Figure 5: for the initial instant $t = 0$ after the partial pressure change the defect concentrations inside the sample are still identical to the previous equilibrium values, and the defect concentrations of the surface layer are equilibrated with the new gas phase composition in which one of the pressures is kept constant). Using a boundary condition $\nabla\mu_{H_2O} = 0$ corresponds to setting the second term $(\partial\mu_O/\partial c_H)\nabla c_H$ in Equation (12) to zero which is not correct for the general case. One consequence is that some of the diffusion coefficients defined in this way can attain values that are significantly outside the expected limits (cf. also Figure 1): $\tilde{D}_{vH}$ meant to describe $V_O^{\bullet\bullet}$ diffusion after p_{H_2O} change can drastically drop below $D_{V_O^{\bullet\bullet}}$ for high hole concentration; on the other hand $\tilde{D}_{iO}$ associated with proton diffusion after p_{O_2} change can exceed $D_{h^{\bullet}}$. For a more detailed discussion see Part II of a previous study by Poetzsch et al.[19]

4. Exemplary Numerical Results for p_{H_2O} Changes

We focus here on p_{H_2O} changes, for which a two-component relaxation was observed experimentally.[10–13] A detailed

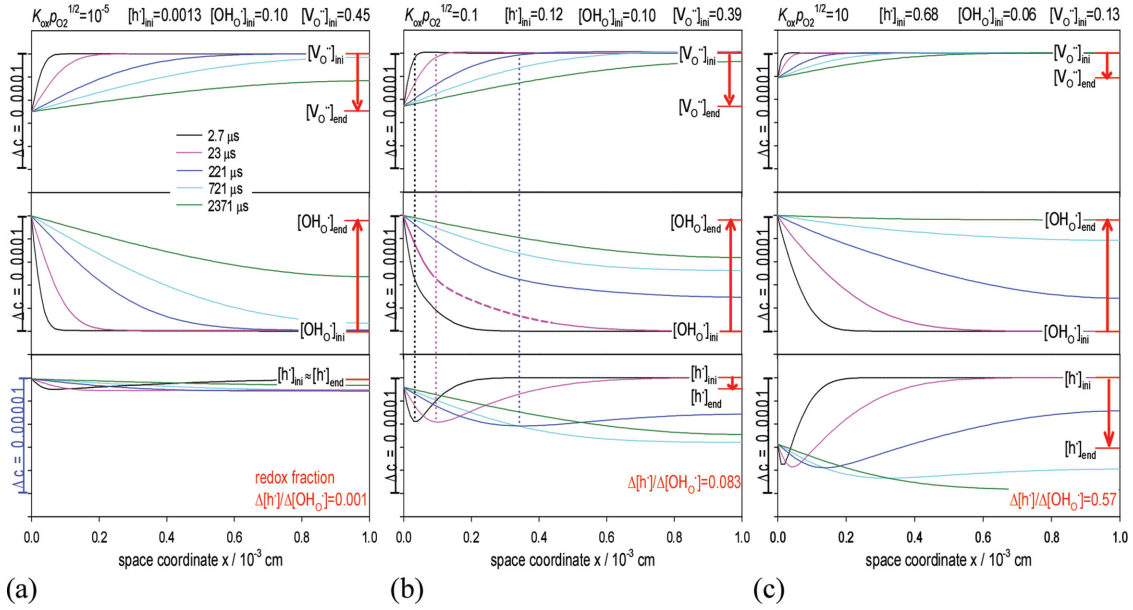

Figure 6. Space-resolved concentration profiles (the sample surface is located at $x = 0$) for oxygen vacancies (top), protons (middle), and holes (bottom) at different times after a stepwise p_{H_2O} increase. They are simulated for a) low, b) intermediate, and c) high hole concentration, corresponding to a transition from an electrolyte-type material with predominant acid-base thermodynamics to a predominant hole conductor with significant redox fraction. Red arrows show the difference between initial and final defect concentrations. The defect diffusivity ratios are always $D_{h^{\bullet}} = 10^2 D_{OH_O^{\bullet}} = 10^4 D_{V_O^{\bullet\bullet}}$. The "moving boundary phenomenon" observed at intermediate hole concentrations is related to the striking changes in slope in the $OH_O^{\bullet}$ concentration profiles which occur at the position of the minimum in $[h^{\bullet}]$ as indicated by the vertical dotted lines in b). This slope change is also exemplarily emphasized by the change from solid to dashed line style for the pink line in b).

numerical evaluation – including p_{O_2} changes – is beyond the scope of the present investigation, but will be given in a forthcoming paper.[19] We concentrate on two aspects which were discussed already in the theoretical section, and which cannot be reproduced by the semiquantitative model of two independent diffusion processes: (i) The transition from onefold water uptake to twofold relaxation on increasing hole concentration (realized by varying $K_O p_{O_2}^{1/2}$). (ii) The fact that even the proton uptake can comprise two stages with different effective diffusivities (initial fast hydrogen uptake, followed by slower uptake of water, Figure 6b), and the closely related "moving boundary" phenomenon. The surface reaction is assumed to be infinitely fast, and $D_{h^{\bullet}} \geq D_{OH_O^{\bullet}} \geq D_{V_O^{\bullet\bullet}}$ unless stated else (to assess the fundamental characteristics of the relaxation, only the ratios of defect diffusivities are important). Computational details are given in Appendix 1.

Figure 6 shows space-resolved defect concentration profiles developing after a p_{H_2O} increase for three prototypical materials with low, intermediate, and high $[h^{\bullet}]$ visualizing the drastic changes in relaxation kinetics with increasing $[h^{\bullet}]$ that were semiquantitatively predicted in Figure 5a.

As discussed in Figure 3, for materials with comparably low hole concentration, the overall reaction will essentially be water uptake (as in $Ba(Zr_{1-x}Y_x)O_{3-\delta}$[13,20] where stoichiometry changes due to oxygen exchange reaction (1) are still very small).[38] According to Figure 5a, for such a material onefold relaxation is expected. Correspondingly, the concentration profiles in Figure 6a do not exhibit any peculiar features and have identical time constants for protons and oxygen vacancies. The transient changes in $[h^{\bullet}]$ are still tiny. The integral defect concentrations (integrated over the whole sample) exhibit a onefold time dependence (**Figure 7**a, the $t^{1/2}$ scaling allows us to directly determine the respective diffusion coefficients from the linear region). This curve exactly corresponds to the analytical solution of Fick's law yielding $D^{\delta}_{H_2O}$ which varies in-between $D_{OH_O^{\bullet}}$ for low and $D_{V_O^{\bullet\bullet}}$ for high degree of hydration.[6]

With increasing $[h^{\bullet}]$, corresponding to Figures 6b and 7b, the overall reaction is still predominantly water uptake (the overall redox fraction defined as $-\Delta[h^{\bullet}]/\Delta[OH_O^{\bullet}]$ remains below 10%). Nevertheless, the material moves into the twofold regime (red area in Figure 5a). The discrepancy between the ratio of initial $V_O^{\bullet\bullet}$ and $h^{\bullet}$ fluxes (to compensate the fast $OH_O^{\bullet}$ uptake) and the ratio of overall $V_O^{\bullet\bullet}$ and $h^{\bullet}$ uptake required by equilibrium thermodynamics is also illustrated by the arrows atop Figure 7. Several closely interrelated changes occur. The evolution of proton and $V_O^{\bullet\bullet}$ concentration profiles occurs with different time constants (much deeper penetration of the $[OH_O^{\bullet}]$ profile compared to $[V_O^{\bullet\bullet}]$), as also shown in the integrated concentration changes in Figure 7b. The effective diffusion coefficients D^{eff}_H of hydrogen in this first stage of the relaxation is about 10 times higher than D^{eff}_O for oxygen, corresponding to largely decoupled transport of H and O. D^{eff}_H takes values in-between $D_{OH_O^{\bullet}}$ and $D^{\delta}_{H_2O}$, i.e., proton uptake at the expense of holes proceeds faster than hypothetical proton uptake ambipolarly coupled to the filling of $V_O^{\bullet\bullet}$ (red $D^{\delta}_{H_2O}$ curve in Figure 7b). On the other hand D^{eff}_O is in-between $D^{\delta}_{H_2O}$ and $D_{V_O^{\bullet\bullet}}$, i.e., oxygen uptake (and thus the completion of the overall relaxation process) is now slower than in the case of chemical diffusion of water (onefold kinetics). Driven by the requirement to supply charge compensation for the fast proton

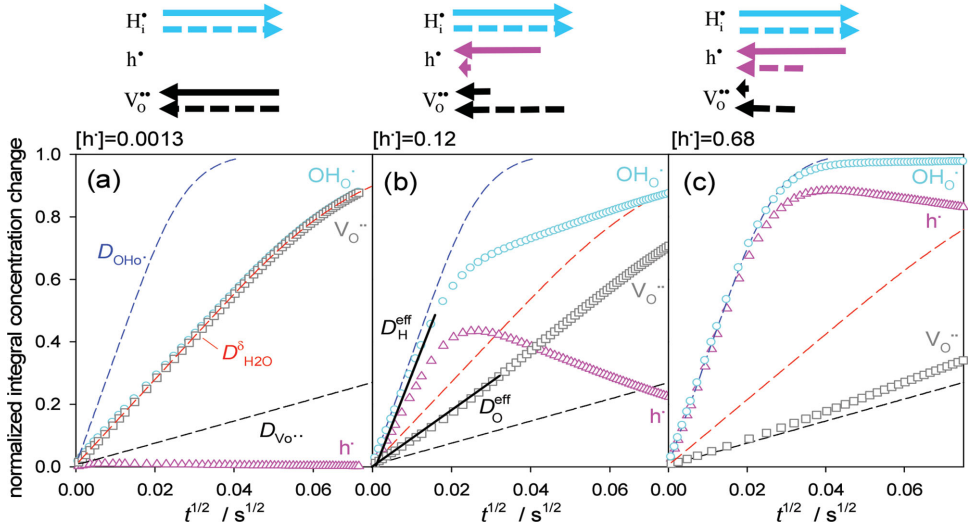

Figure 7. a) Normalized integral $V_{\ddot{O}}$, $OH_{\dot{O}}$, $h^{\bullet}$ concentration changes (symbols) versus square root of time after p_{H_2O} increase for low, intermediate, and high $[h^{\bullet}]$ as in Figure 6. Dashed lines correspond to $D_{V_{\ddot{O}}}$, $D_{OH_{\dot{O}}}$, and hypothetical $D^{\delta}_{H_2O}$ (simulated with immobile $h^{\bullet}$), black straight lines in b) to D^{eff}_{H} and D^{eff}_{O}. c) $[OH_{\dot{O}}]$ and $[V_{\ddot{O}}]$ are normalized according to $M_k = (c_k(t) - c_k(t=0))/(c_k(t=\infty) - c_k(t=0))$; for convenience $[h^{\bullet}]$ is normalized to the overall proton uptake $([h^{\bullet}(t)] - [h^{\bullet}(t=0)])/([OH_{\dot{O}}(t=0)] - [OH_{\dot{O}}(t=\infty)])$. This results in positive normalized concentration changes for all three defects, despite the fact that after p_{H_2O} increase, $[V_{\ddot{O}}]$ decreases while $[h^{\bullet}]$ exhibits a nonmonotonic fast decrease followed by slower partial recovery (cf. Figures 6 and A1 in Appendix 1). The initial $OH_{\dot{O}}$, $V_{\ddot{O}}$, and $h^{\bullet}$ fluxes ($t = 0$, $x = 0$) are schematically shown at the top as solid arrows, the overall composition changes (thermodynamics) are indicated by dashed arrows.

uptake, the transient decrease of $[h^{\bullet}]$—corresponding to a transient reduction of the sample—becomes very pronounced and strongly exceeds the overall $\Delta[h^{\bullet}]$. Only by the slow reoxidation (required to complete the overall thermodynamic reaction), the hole concentration largely comes back to its initial value. This nonmonotonic behavior is observed for the integrated hole concentration (Figure 7b) as well as for $[h^{\bullet}]$ at any given locus during the temporal evolution of the concentration profiles (Figure 6b). It is interesting to note that after the hole concentration change has passed its maximum, some further proton uptake occurs, but now with a lower effective diffusivity (linear region in Figure 7b at large times with smaller slope) and compensated by $V_{\ddot{O}}$ annihilation, not $h^{\bullet}$ consumption.

Finally, Figures 6c and 7c show an example of high $[h^{\bullet}]$. These conditions are located close to the singlefold H uptake region in the materials map Figure 5a. For these conditions, the overall redox fraction strongly increases to 57% (the relation between hole concentration, redox fraction, and degree of decoupling will be discussed in Poetzsch et al. in more detail).[19] The effective H diffusivity D^{eff}_{H} in the first stage of the relaxation is identical to $D_{OH_{\dot{O}}}$ (proton uptake almost exclusively compensated by holes corresponds to chemical diffusion of hydrogen, and for high $h^{\bullet}$ concentration and mobility, $D^{\delta}_{H} \approx D_{OH_{\dot{O}}}$). D^{eff}_{O} comes close to $D_{V_{\ddot{O}}}$, leading to very strong decoupling with $D^{eff}_{H}/D^{eff}_{O} \approx 0.7 \cdot D_{OH_{\dot{O}}}/D_{V_{\ddot{O}}}$. The slower reoxidation process slightly increases $[h^{\bullet}]$ after the maximum transient reduction, but in accordance with the high redox fraction the final hole concentration strongly differs from the initial value, and the annihilation of $V_{\ddot{O}}$ contributes only to a minor part to the charge compensation for proton uptake.

After having discussed the changes from onefold to twofold and back to onefold kinetics on increasing $[h^{\bullet}]$ (via increasing $K_O p_{O_2}^{1/2}$, see Figure 5a), let us now inspect in more details the phenomena of different D^{eff}_{H} in the initial and later stage of the relaxation and the closely related "moving boundary" phenomenon, which arise in particular in the twofold kinetics regime. These features originate from the fact that H and O diffusion are not independent processes. This is obvious from Equations (18)–(32) in which the flux of one species is driven by two concentration gradients which are not related by a simple proportionality, and consequently also manifests itself in the simulation results. In the time evolution of integral concentration changes in Figure 7b, the effective H diffusivity at long times (after the maximum transient $[h^{\bullet}]$ change) is obviously lower than in the initial stage. The variation in the effective H diffusivity is also clearly visible in the space-resolved concentration profiles, e.g., Figure 6b. For short to moderate times, the proton profiles (e.g., pink line in Figure 6b) cannot be described by a single diffusion coefficient throughout the sample: the profile consists of a steeper initial part (bold) and a flatter section deeper inside the sample (bold dashed line), cf. also the slopes of the proton profile in Appendix 3. Since a steeper concentration profile corresponds to a lower diffusivity, this reflects that at a given time hydrogen diffusion occurs with different effective diffusivities in these two parts of the sample. The lower diffusivity region extends from the surface up to the location where $[h^{\bullet}]$ takes its minimum value (zone already being reoxidized, cf. the $[V_{\ddot{O}}]$ profile), the higher diffusivity is found in the inner region of the sample. The boundary between the regions is defined by the minimum in $[h^{\bullet}]$, which moves further into the sample with increasing time, and eventually vanishes at large times. This behavior, which arises here simply from the coupling of the three defects according to Equations (18)–(32), naturally explains the "moving boundary" situation which had

to be heuristically implemented into preceding phenomenological simulations to properly describe the concentration profiles arising in slightly Fe-doped $SrTiO_3$ single crystals after a p_{H_2O} change.[12]

The fact that the minimum in [h•] marks the boundary between the regions with different effective H diffusivities can be understood, e.g., from Equation (30) giving the proton flux as function of the gradients in proton and hole concentration. While $D^{H}_{H(h)}$ in the first term is always positive, in the second term $t_{H_i}(D_{V_O^{\cdot\cdot}} - D_{h^{\cdot}})$ has a negative sign owing to $D_{h^{\cdot}} > D_{V_O^{\cdot\cdot}}$. Thus, close to the surface where ∇c_{H_i} has the same sign as $\nabla c_{h^{\cdot}}$ the proton flux is decreased by the influence of the hole gradient, while deeper in the sample it is accelerated by $\nabla c_{h^{\cdot}}$ having the opposite sign there. This observation of different effective hydrogen diffusivities in the outer and inner region of the sample also explains why even for a large $D_{OH_O^{\cdot}}/D_{V_O^{\cdot\cdot}}$ ratio and hole concentration the transient reduction of the sample often remains incomplete, i.e., the transient $\Delta[h^{\cdot}]$ is smaller than the overall $\Delta[OH_O^{\cdot}]$ (more examples can be found in Poetzsch et al.)[19] The lower effective hydrogen diffusivity in the growing outer (reoxidized) zone acts as a throttle valve for hydrogen supply to the inner zone with high diffusivity, and limits the maximum transient reduction developed in the sample.

All these observations clearly indicate that the approximation of independent diffusion of H and O (complete decoupling, corresponding to an independent diffusion of both components into a homogeneous medium) is insufficient for a complete and quantitatively correct description. The entire relaxation behavior cannot be reproduced with a set of only one hydrogen and oxygen diffusivity such as $\tilde{D}_{iH}, \tilde{D}_{vH}$ upon a p_{H_2O} change as suggested by Kim and Yoo[13] (or with any other set of a single D^{eff}_{H} and D^{eff}_{O}); such procedures must remain semiquantitative approximations for the first stage of the overall relaxation process. The peculiar relaxation behavior has its origin in the fact that the flux of one particle is always related to two concentration gradients (cf. Equation (21)), allowing for uphill diffusion in terms of its own concentration gradient (such as the pronounced transient reduction, i.e., nonmonotonic hole concentration change of the sample although the overall reaction requires only a tiny change in [h•]) and space-dependent effective diffusivities (e.g., for protons, corresponding to the "moving boundary" phenomenon). While in two-carrier systems nonconstant chemical diffusivities occur only under large driving forces,[14] these features arise here already for small driving forces simply due to the fact that the presence of a third carrier relaxes the otherwise strict direct mutual coupling of two carrier concentrations (and their gradients) by the electroneutrality condition.

5. Relevance for Functional Materials

In the present publication the effects of three carriers contributing to stoichiometry relaxation are exemplified for the case of an oxide containing protons, oxygen vacancies, and holes and the experimental examples given largely refer to electrolyte (acceptor-doped (Ba,Sr)(Zr,Ce,Sn,In)O_3) and electrode materials (Mn-, Fe-, and Co-based mixed conducting perovskites) for proton conducting ceramic fuel cells, as well as to ceramic hydrogen permeation membranes. Clearly, for these materials a detailed understanding in terms of their complex defect chemistry and transport properties is essential in constructing efficient devices (suppression of electronic leakage in the electrolyte materials, but desired mixed electronic/protonic conductivity for electrodes, permeation membranes). The understanding of the three-carrier problem is absolutely crucial for understanding the functionality, and optimizing performance. A striking example was the surprising observation of nonmonotonic effects in the kinetics of stoichiometry changes in $SrTiO_3$.[10]

However, similar situations can arise in a large number of other ionic solids, many of which are important functional materials. First, we want to emphasize that protons are found in many more oxides (e.g., zirconia,[39] ceria,[40] titania,[41] zinc oxide),[42] and that owing to their larger mobility (in particular at low temperature) compared to other defects such as oxygen vacancies they may affect the conductivity and concentration of other point defects even if present in small concentrations. Here it is important to emphasize again that proton uptake does not necessarily require oxygen vacancies, but that it can also proceed by a redox reaction as described in Equation (3). Oxides such as $SrTiO_3$ and TiO_2[43,44] are intensively explored for memristive switching. So far these investigations focus on the role of electrons and oxygen vacancies, but the presence of some protons is highly plausible, which will react to the applied chemical and/or electrical driving forces.

Furthermore, situations with relevant contributions from three mobile carriers are found without protons being involved. In several functional oxides such as zinc oxide (ab initio calculations[45] and experimental work cited therein), titania,[8] and donor-doped perovskites,[9] in addition to oxygen vacancies also cation interstitials or vacancies contribute significantly to ionic transport under certain conditions (where also internal reactions such as the Schottky reactions coupling these defects are not in equilibrium). Together with electronic carriers, again we encounter a three carrier situation. Also if the ionic conductivity of one carrier is comparatively small, it would be grossly wrong to neglect it in terms of long-time behavior. It can be anticipated that various ageing phenomena may be explained by such kinetics.[2,46–48]

Thus, a quantitatively precise description of the kinetics of chemical composition change, not only in simplified limiting cases but in particular in the complex intermediate situations, as treated in the present publication is of outmost importance.

6. Summary

Systems with three carriers (in this study: protons, oxygen vacancies, and electron holes) can exhibit a complex behavior with respect to equilibrium thermodynamics and diffusion kinetics after p_{H_2O} and p_{O_2} changes. According to the defect chemical model the overall reaction after p_{H_2O} increase (at constant p_{O_2}) changes from predominant water uptake in materials with $[h^{\cdot}] < [V_O^{\cdot\cdot}]$ to mainly hydrogen incorporation for $[h^{\cdot}] > [V_O^{\cdot\cdot}]$ (with the relative magnitude of the defect concentrations depending on K_O, K_W).

For the kinetics of stoichiometry changes, exact diffusion equations are derived (assuming negligible defect interactions). Mutual coupling of the defect concentrations by local electroneutrality combined with the additional degree of freedom provided by the presence of a third carrier leads to complex situations that even allow for "uphill diffusion" of a carrier relative to its own concentration gradient. To completely describe the system, four diffusion coefficients are required. While the direct diffusivity terms are isomorphic (but not identical) to chemical diffusivities in a two carrier system, the indirect terms contain differences of defect diffusivities. The relaxation after p_{H_2O} change can be onefold (e.g., chemical diffusion of water) or twofold (decoupled into fast H incorporation followed by slower O uptake, leading to pronounced nonmonotonic concentration changes for holes) depending on concentration and mobility of electronic carriers. In a defect-chemical map of materials, the region of twofold water uptake is unambiguously identified from the combination of thermodynamic and kinetic considerations.

Numerical simulations are required for a detailed analysis of the resulting relaxation kinetics. They visualize the analytical relations, confirm the results and highlight important details. A special feature is the nonmonotonic change of one carrier concentration acting as a kinetic intermediate. Furthermore, under conditions of twofold relaxation the effective H diffusivity is lower in the outer part of the sample. This naturally explains the experimentally observed "moving boundary" phenomenon, and indicates that simplistic approaches based on diffusion in a homogeneous medium are insufficient for a complete quantitative analysis.

Appendix 1: Computational Details

Inserting the electroneutrality condition $[A'] = 2[V_O^{\cdot\cdot}] + [OH_O^{\cdot}] + [h^{\cdot}]$ with acceptor concentration $[A'] = 1$ and oxygen site balance $3 = [O_O^x] + [V_O^{\cdot\cdot}] + [OH_O^{\cdot}]$, the mass action constants (1) and (2) lead to an implicit equation for the $V_O^{\cdot\cdot}$ concentration

$$p_{O_2}^{1/2} K_O = \frac{(3-[V_O^{\cdot\cdot}]-[OH_O^{\cdot}])([A']-2[V_O^{\cdot\cdot}]-[OH_O^{\cdot}])^2}{[V_O^{\cdot\cdot}]} \quad (33)$$

where the proton concentration is given by

$$[OH_O^{\cdot}] = \frac{-[V_O^{\cdot\cdot}]p_{H_2O}K_W + \sqrt{([V_O^{\cdot\cdot}]p_{H_2O}K_W)^2 - 4p_{H_2O}K_W[V_O^{\cdot\cdot}]([V_O^{\cdot\cdot}]-3)}}{2} \quad (34)$$

Defect concentrations were calculated numerically from Equations (33) and (34) using Matlab. Component partial pressures p_{H_2O} and p_{O_2} are normalized to 1 bar. The derivatives $\partial c_{defect}/\partial \ln p$ in Figure 2 are calculated as $\Delta c_{defect}/\Delta \ln p$ with a 10% change in partial pressure.

For the calculation of the initial fluxes in Figure 5, a value of $\nabla\mu_{H_2O}$ (or $\nabla\mu_O$) is arbitrarily chosen since it appears identically in all defect fluxes and only the relative magnitude of the fluxes is decisive (however, to be consistent with the boundaries between the different reactions derived from small perturbation of equilibrium thermodynamics according to Equations (4) and (5), Figure 5 implicitly assumes $\nabla\mu_{H_2O}$ or $\nabla\mu_O$ to be comparably small). Conductivities and transference numbers are obtained from defect concentrations and mobilities, the hole flux is obtained from the electroneutrality condition Equation (8).

The relaxation after p_{H_2O} changes were simulated under the assumption of infinitely fast surface exchange reactions, i.e., the defect concentrations in the first layer of the material immediately assume their new equilibrium values (calculated from the defect model). The one-dimensional symmetrical diffusion into the sample from both sides was then simulated by finite difference calculations performed using Matlab. The sample thickness was chosen to be $l = 0.002$ cm divided into compartments of width $\Delta l = 10^{-5}$ cm (since the surface reaction is assumed infinitely fast, the actual length does not have any influence on the trends in relaxation kinetics). For the calculations concentration-independent diffusion coefficients were used, i.e., from Equations (18) and (19) the diffusion coefficients and cross terms $D^V_{V(H)}$, $D^H_{H(V)}$, $D^V_{H(V)}$, $D^H_{V(H)}$ were calculated at the beginning for the initial defect concentrations and transference numbers and then used throughout the simulation. Test calculations with these diffusivities depending on the local defect concentrations via local t_k in Equations (18) and19) in Poetzsch et al.[19] show that this approximation does not affect the results. This is to be expected for moderate p_{H_2O} and p_{O_2} changes because the defect transference numbers in Equations (18) and (19) will hardly differ between initial, transient, and final stages of the relaxation. The flux of $V_O^{\cdot\cdot}$ and $OH_O^{\cdot}$ between compartments i and $i+1$ during time increment Δt was calculated according to Equations (18) and (19) from

$$J_{V_O^{\cdot\cdot},i\to i+1} = -D^V_{V(H)}\frac{[V_O^{\cdot\cdot}]_{i+1}-[V_O^{\cdot\cdot}]_i}{\Delta l} - 0.5D^V_{H(V)}\frac{[OH_O^{\cdot}]_{i+1}-[OH_O^{\cdot}]_i}{\Delta l} \quad (35)$$

$$J_{H_i^{\cdot},i\to i+1} = -2D^H_{V(H)}\frac{[V_O^{\cdot\cdot}]_{i+1}-[V_O^{\cdot\cdot}]_i}{\Delta l} - D^H_{H(V)}\frac{[OH_O^{\cdot}]_{i+1}-[OH_O^{\cdot}]_i}{\Delta l} \quad (36)$$

The concentrations are then updated according to

$$\Delta[V_O^{\cdot\cdot}] = \frac{\Delta t}{\Delta l}\cdot(J_{V_O^{\cdot\cdot},i-1\to i} - J_{V_O^{\cdot\cdot},i\to i+1}) \quad (37)$$

$$\Delta[OH_O^{\cdot}] = \frac{\Delta t}{\Delta l}\cdot(J_{OH_O^{\cdot},i-1\to i} - J_{OH_O^{\cdot},i\to i+1}) \quad (38)$$

(cf. similar procedure in Merkle et al.)[14] The hole concentration is obtained from the electroneutrality condition. In the present study, the time increments were increased in 4–5 steps during the simulation to obtain concentration profiles with good time resolution in the initial stage, while larger increments suffice towards the end. As long as the changes are sufficiently small, the magnitude of the concentration change (typically, Δc did not exceed 10^{-4}) does not affect the shape of the concentrations profiles.[19] For situations where the relaxation can properly be described by a single diffusion coefficient,

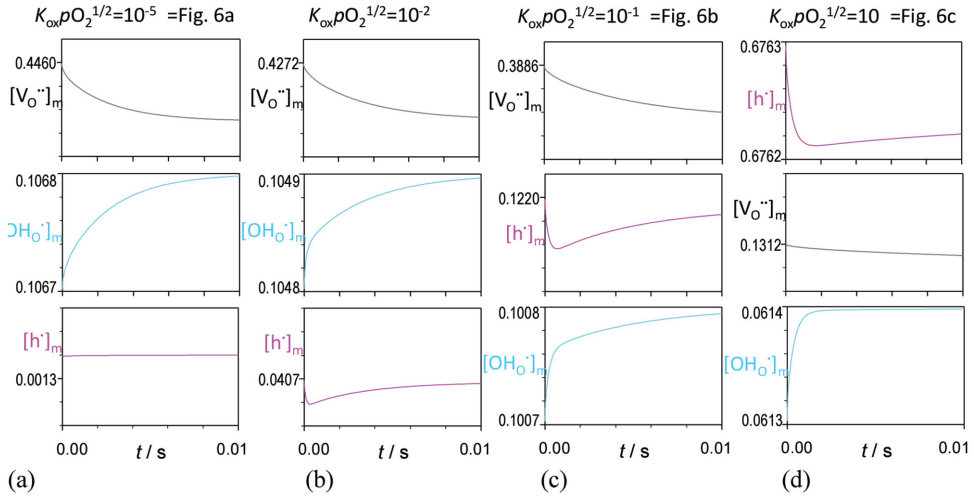

Figure A1. Time dependence of integrated (mean) defect concentrations after stepwise p_{H_2O} increase for different values of $K_O p_{O_2}^{1/2}$ corresponding to different [h•]. The interval between two minor ticks on the *y*-axis always corresponds to $\Delta c = 2 \times 10^{-5}$. a,c,d) have the same input parameters as a), b), and c) in Figures 6 and 7. The evolution of [h•] in Figure A1b illustrates that a nonmonotonic relaxation behavior appears already for [h•] < [$OH_O^{\cdot}$].

the obtained concentration profiles and time dependence agree with the available analytical solutions (cf. the plots of normalized integral defect concentration in Section 4 yielding straight lines with the expected slopes). Space-dependent concentration profiles are given in Figure 6, the time dependence of the integrated concentrations in **Figure A1**.

Effective diffusivities D_O^{eff} and D_H^{eff} for O and H were extracted from the slope of the linear region in plots of normalized concentration changes versus $t^{1/2}$ (Figure 7) according to $D = (\text{slope})^2 \pi l^2/16$.[49] Concentration profiles corresponding to chemical diffusion in a two-carrier situation ($D_O^{\delta}, D_H^{\delta}, D_{H_2O}^{\delta}$) were obtained for the same initial defect concentrations, setting the mobility of the third defect to zero and choosing appropriate concentration changes ($\Delta[h^{\cdot}] = -2\Delta[V_O^{\cdot\cdot}]$ for D_O^{δ}, $\Delta[h^{\cdot}] = -\Delta[OH_O^{\cdot}]$ for D_H^{δ}, $\Delta[OH_O^{\cdot}] = -2\Delta[V_O^{\cdot\cdot}]$ for $D_{H_2O}^{\delta}$; thus, they represent to some degree hypothetical quantities, e.g., pure water uptake for a material which according to its high [h•] would exhibit a nonnegligible contribution of H uptake by redox reaction). The hole concentration is varied in a series of simulations by inserting different $K_O p_{O_2}^{1/2}$ values into the defect model at fixed $K_W p_{H_2O}$ and acceptor concentration [A′] = 1.

In order to assess the fundamental characteristics of the relaxation process (singlefold versus twofold kinetics; ratio of proton versus $V_O^{\cdot\cdot}$ flux) only the ratios of defect diffusivities are important. Their absolute values, as well as absolute sample dimensions are not relevant and can be arbitrarily chosen. Unless stated else $D_{h^{\cdot}} \geq D_{OH_O^{\cdot}} \geq D_{V_O^{\cdot\cdot}}$ is assumed, motivated by the properties of acceptor-doped perovskites such as $Ba(Zr_{1-x}Y_x)O_{3-\delta}$,[20,25] $SrTiO_3$,[50,51] or SOFC cathode materials.[52–54] As realistic example, we chose $D_{V_O^{\cdot\cdot}} = 10^{-5}$ cm^2 s^{-1}, $D_{OH_O^{\cdot}} = 10^{-3}$ cm^2 s^{-1}, $D_{h^{\cdot}} = 10^{-1}$ cm^2 s^{-1}. Sets of defect concentrations (corresponding to different materials, or one material in a very large p_{O_2} and/or *T* range) are obtained from the defect model by varying $K_O p_{O_2}^{1/2}$ keeping $K_w p_{H_2O} = 0.01$ constant. While this variation affects all defects (the ratio $[V_O^{\cdot\cdot}]/[OH_O^{\cdot}]$ is about 4 for the largest $K_O p_{O_2}^{1/2}$ and approaches 1 for the lowest $K_O p_{O_2}^{1/2}$ values covered here), the largest relative changes occur for [h•] which increases from 10^{-4} to almost 1. This transforms the material from a $OH_O^{\cdot}/V_O^{\cdot\cdot}$ conducting electrolyte at lowest [h•] to a sample with predominant hole conduction (but still perceptible concentration of mobile $V_O^{\cdot\cdot}$ and $OH_O^{\cdot}$).

Appendix 2: Initial Fluxes for Different Defect Mobility Ratios

It is obvious that the width of the twofold region is related to the ratio of the respective compensating defect diffusivities, e.g., $D_{h^{\cdot}} / D_{V_O^{\cdot\cdot}} = 10^4$ yields a wider twofold zone for relaxation after p_{H_2O} changes compared to $D_{OH_O^{\cdot}} / D_{V_O^{\cdot\cdot}} = 10^2$ for p_{O_2} changes in Figure 5. **Figure A2** compares the initial fluxes calculated from Equation (11) for different defect diffusivity ratios. In the middle column, $D_{h^{\cdot}}$ is decreased while in the right column $D_{OH_O^{\cdot}}$ is decreased relative to Figure 5. In all cases, the thermodynamically determined boundary (between twofold and onefold H uptake for p_{H_2O} change, and between twofold and onefold H release for p_{O_2} change) remains unaffected. A decreased hole mobility in Figure A2b leads to a smaller twofold region (the surface describing the hole flux is lowered compared to the $V_O^{\cdot\cdot}$ flux, shifting the intersection which defines the left boundary of the twofold regime to the right). But only at $D_{h^{\cdot}} = D_{V_O^{\cdot\cdot}}$ the twofold region vanishes (cf. the first term in Equation (19) becoming zero). Interestingly, a decreased proton mobility (Figure A2c) does not change the extent of the region where in principle twofold relaxation occurs (although it will affect the magnitude of decoupling) because a lower $D_{OH_O^{\cdot}}$ does not affect the relative magnitude of $h^{\cdot}$ and $V_O^{\cdot\cdot}$ flux (the intersection of which defined the boundary). It is noteworthy that also for $D_{V_O^{\cdot\cdot}} = D_{OH_O^{\cdot}}$ in Figure A2c twofold behavior is predicted as soon as the material exhibits a sufficiently high [h•] to develop a perceptible redox fraction, which means that a part of the proton uptake is compensated by holes (fast process) but the other part by $V_O^{\cdot\cdot}$ (slower). However, the difference between D_O^{eff} and D_H^{eff}

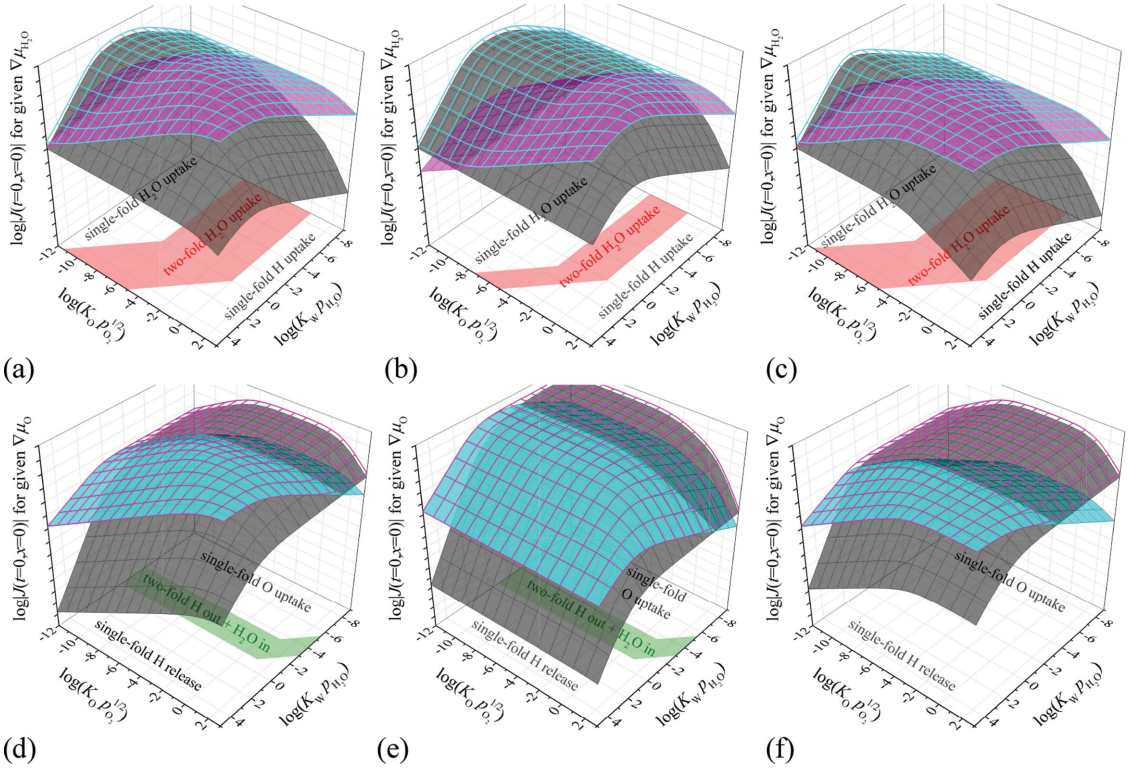

Figure A2. Initial fluxes J_{ini} of $OH_{\ddot{O}}^{\bullet}$ (light blue surface or mesh), $V_{\ddot{O}}^{\ddot{}}$ (grey surface), and $h^{\bullet}$ (pink surface or mesh); absolute values, in arbitrary units, calculated from Equation (11). Top row: after p_{H_2O} increase, bottom: after p_{O_2} increase. a,d) $D_{V_{\ddot{O}}^{\ddot{}}} = 10^{-5}$ cm^2 s^{-1}, $D_{OH_{\ddot{O}}^{\bullet}} = 10^{-3}$ cm^2 s^{-1}, $D_{h^{\bullet}} = 10^{-1}$ cm^2 s^{-1}. b,e) $D_{V_{\ddot{O}}^{\ddot{}}} = 10^{-5}$ cm^2 s^{-1}, $D_{OH_{\ddot{O}}^{\bullet}} = D_{h^{\bullet}} = 10^{-3}$ cm^2 s^{-1}. c,f) $D_{V_{\ddot{O}}^{\ddot{}}} = 10^{-5} = D_{OH_{\ddot{O}}^{\bullet}} = 10^{-5}$ cm^2 s^{-1}, $D_{h^{\bullet}} = 10^{-1}$ cm^2 s^{-1}.

is moderate, and the transient reduction is close to the overall redox fraction (i.e., there is not much "overshooting" of the hole concentration).

For p_{O_2} changes, a decreased $D_{h^{\bullet}}$ does not affect the width of the twofold region (Figure A2e). On the other hand, a decreased $D_{OH_{\ddot{O}}^{\bullet}}$ shifts the intersection of the proton and $V_{\ddot{O}}^{\ddot{}}$ surfaces to the left, eventually leading to a vanishing of the twofold zone (Figure A2f).

Based on the initial fluxes consideration, the twofold zone vanishes when the two compensating defects ($V_{\ddot{O}}^{\ddot{}}$ and $h^{\bullet}$ in case of p_{H_2O} change, $V_{\ddot{O}}^{\ddot{}}$ and $OH_{\ddot{O}}^{\bullet}$ in case of p_{O_2} change) have the same mobility. On the other hand, $J_{V_{\ddot{O}}^{\ddot{}}}$ and $J_{OH_{\ddot{O}}^{\bullet}}$ in Equations (18) and (19) consist of a single term only (which is the sufficient condition for onefold kinetics) only when $D_{OH_{\ddot{O}}^{\bullet}} = D_{V_{\ddot{O}}^{\ddot{}}} = D_{h^{\bullet}}$. However, numerical simulations show that still $D_O^{eff} \approx D_H^{eff}$. This can be understood from the fact that in case of $D_{V_{\ddot{O}}^{\ddot{}}} = D_{h^{\bullet}}$ (for p_{H_2O} change), independent of the $D_{OH_{\ddot{O}}^{\bullet}}$ value the ratio of the initial H and O fluxes calculated from Equation (11) is very similar to the overall (equilibrium) H and O uptake, and thus in this particular situation the $OH_{\ddot{O}}^{\bullet}$ and $V_{\ddot{O}}^{\ddot{}}$ concentration gradients are directly proportional to each other (during the whole relaxation) leading to onefold relaxation.

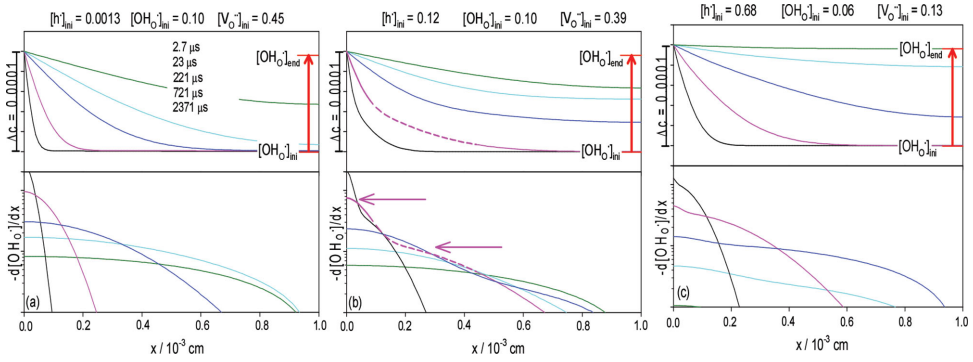

Figure A3. Spatial proton concentration profiles and their derivatives $d[OH_O^{\bullet}]/dx$ for a) low, b) intermediate, and c) high $[h^{\bullet}]$ (same parameters as in Figure 6). The pink arrows in b) indicate the two regions of higher and lower slopes in the pink proton profile.

Appendix 3: Slope of Spatial Proton Profiles for "Moving Boundary Phenomenon"

Figure A3a shows the derivative $d[OH_O^{\bullet}]/dx$ of the proton profiles for low, intermediate, and high $[h^{\bullet}]$, to give a more quantitative impression of the characteristic change in the slope of $[OH_O^{\bullet}]$. For low $[h^{\bullet}]$ corresponding to singlefold relaxation (Figure A3a) the whole profile can be described by a single diffusion coefficient, and correspondingly the slopes of the proton profiles decrease smoothly without any special features. In particular for kinetics in the twofold regime (Figure A3b) two plateaux in the derivative—corresponding to an approximately stepwise change of the slope—are visible, which indicate the regions with low (close to the surface) and high (deeper inside the sample) effective H diffusivity. The boundary between these regions is given by the location of the $[h^{\bullet}]$ minimum, and penetrates deeper into the sample with increasing time. For materials with high $[h^{\bullet}]$ (Figure A3c) the difference in effective H diffusivity in the sample's inner and outer part becomes less pronounced (the proton profile in Figure 6c smoothly follows the usual shape, without the visible kink as in Figure 6b) because the decreasing $t_{H_i^{\bullet}}$ decreases the second term in Equation (30) which causes that difference.

Received: July 4, 2014
Revised: December 19, 2014
Published online: February 10, 2015

[1] I. Riess, *Solid State Ionics* **2003**, *157*, 1.
[2] M. Martin, *J. Chem. Thermodyn.* **2003**, *35*, 1291.
[3] C. Wagner, W. Schottky, *Z. Phys. Chem.* **1930**, *B11*, 163.
[4] C. Wagner, *Prog. Sol. St. Chem.* **1975**, *10*, 3.
[5] R. Waser, *Ber. Bunsenges. Phys. Chem.* **1986**, *90*, 1223.
[6] K. D. Kreuer, E. Schönherr, J. Maier, *Solid State Ionics* **1994**, *70*, 278.
[7] J. Maier, *J. Am. Ceram. Soc.* **1993**, *76*, 1212.
[8] D.-K. Lee, H.-I. Yoo, *Solid State Ionics* **2006**, *177*, 1.
[9] H.-I. Yoo, C.-E. Lee, *J. Am. Ceram. Soc.* **2005**, *88*, 617.
[10] J. H. Yu, J.-S. Lee, J. Maier, *Angew. Chemie Int. Ed.* **2007**, *46*, 8992.
[11] H.-I. Yoo, J.-Y. Yoon, J.-S. Ha, C.-E. Lee, *Phys. Chem. Chem. Phys.* **2008**, *10*, 974.
[12] J. H. Yu, J.-S. Lee, J. Maier, *Solid State Ionics* **2010**, *181*, 154.
[13] E. Kim, H.-I. Yoo, *Solid State Ionics* **2013**, *252*, 132.
[14] R. Merkle, J. Maier, K. D. Becker, M. Kreye, *Phys. Chem. Chem. Phys.* **2004**, *6*, 3635.
[15] a) D. Poetzsch, R. Merkle, J. Maier, *Phys. Chem. Chem. Phys.* **2014**, *16*, 16446; b) In proton conducting oxides one typically refers mechanistically to protonic defects $OH_O^{\bullet}$ (OH^- instead of O^{2-}) giving rise to proton transfer from one oxide ion to the next, i.e., only the proton migrates, not the entire hydroxide ion. Alternatively the notation $H_i^{\bullet}$ is used to characterize the protonic defect. Later we will use this notation when we refer to kinetics for simplicity, and also to avoid the fallacy that the whole hydroxide ion OH^- would be transported.
[16] A. V. Virkar, *Solid State Ionics* **2001**, *140*, 275.
[17] M. D. Sanders, R. P. O'Hayre, *J. Membr. Sci.* **2011**, *376*, 96.
[18] Y. Liu, X. Tan, K. Li, *Catal. Rev.* **2006**, *48*, 145.
[19] D. Poetzsch, R. Merkle, J. Maier, unpublished.
[20] K. D. Kreuer, *Solid State Ionics* **1999**, *125*, 285.
[21] T. Norby, *Solid State Ionics* **1999**, *125*, 1.
[22] A. Rothschild, W. Menesklou, H. L. Tuller, E. Ivers-Tiffee, *Chem. Mater.* **2006**, *18*, 3651.
[23] R. Merkle, J. Maier, *Angew. Chemie Int. Ed.* **2008**, *47*, 3874.
[24] A. Grimaud, J. M. Bassat, F. Mauvy, P. Simon, A. Canizares, B. Rousseau, M. Marrony, J. C. Grenier, *Solid State Ionics* **2011**, *191*, 24.
[25] H. I. Ji, B.-K. Kim, J. H. Yu, S.-M. Choi, H.-R. Kim, J.-W. Son, H.-W. Lee, J.-H. Lee, *Solid State Ionics* **2011**, *203*, 9.
[26] D. Poetzsch, R. Merkle, J. Maier, *J. Power Sources* **2013**, *242*, 784. Note that in an actual H-SOFC this undesired hole conductivity is suppressed in the region close to the anode with a low effective p_{O_2}.
[27] F. He, T. Z. Wu, R. R. Peng, C. R. Xia, *J. Power Sources* **2009**, *194*, 263.
[28] D. Han, Y. Okumura, Y. Nose, T. Uda, *Solid State Ionics* **2010**, *181*, 1601.
[29] J. Jamnik, J. Maier, *Phys. Chem. Chem. Phys.* **2001**, *3*, 1668.
[30] D. Poetzsch, R. Merkle, J. Maier, unpublished. An experimental example on $Ba_{0.5}Sr_{0.5}Fe_{0.8}Zn_{0.2}O_{3-\delta}$ perovskite in different P_{O_2} will be published separatelywill be published separately.
[31] W. Schottky, *Halbleiterprobleme I* (Ed: W. Schottky), Vieweg, Braunschweig **1954**.
[32] F. A. Kröger, F. H. Stieltjes, H. J. Vink, *Philips Res. Rep.* **1959**, *14*, 557.
[33] a) J. Maier, *Z. Phys. Chem.* **2012**, *226*, 863; b) Switching from component to defect level is easily possible through the relations $\nabla\mu_O = \nabla\tilde{\mu}_{O^{2-}} - 2\nabla\tilde{\mu}_{e^-}$ and $\nabla\tilde{\mu}_{e^-} = \nabla\tilde{\mu}_{e'} = -\nabla\tilde{\mu}_{h^{\bullet}}$. $\nabla\tilde{\mu}_{O^{2-}} = \nabla\tilde{\mu}_{O_\delta^x - V_{\ddot{O}}} = -\nabla\tilde{\mu}_{V_{\ddot{O}} - O_\delta^x}$.[31,32] The transition from building element values to structure element values succeeds according to $\nabla\tilde{\mu}_{V_{\ddot{O}}-O_\delta^x} = \nabla\tilde{\mu}_{V_{\ddot{O}}} - \nabla\tilde{\mu}_{O_\delta^x} \simeq \nabla\tilde{\mu}_{V_{\ddot{O}}}$. The same procedure is valid for μ instead of $\tilde{\mu}$. Note that this transition involves a change in the statistics, which becomes meaningless if $[V_{\ddot{O}}] << [O_{\ddot{O}}^x] \approx$ const. compare ref. [33] for a precise thermodynamic treatment.
[34] L. Heyne, *Solid State Electrolytes*, (Ed: S. Geller), Springer, Berlin, Germany **1977**.
[35] a) S. R. De Groot, *Nonequilibrium Thermodynamics*, North-Holland, Amsterdam **1962**; b) In previous studies, $J_{O_{\ddot{O}}}$ and J_{H_2O} are expressed with $\nabla\mu_O$ and $\nabla\mu_{H_2O}$ as driving forces.[16,17] In that representation real cross terms appear (fulfilling Onsager's reciprocity relation), indicating that in contrast to the point defects the chemical potentials of O_2 and H_2O in the material are not mutually independent (e.g., they are both related to $[V_{\ddot{O}}]$).
[36] L. Onsager, *Phys. Rev.* **1931**, *37*, 405.
[37] D. K. Kim, H. I. Yoo, *Phys. Rev. Lett.* **2006**, *97*, 255901.
[38] Y. Yamazaki, C.-K. Yang, S. M. Haile, *Scr. Mater.* **2011**, *65*, 102.
[39] S. Stotz, C. Wagner, *Ber. Bunsenges. Phys. Chem.* **1966**, *70*, 781.
[40] N. Sakai, K. Yamaji, T. Horita, H. Yokokawa, Y. Hirata, S. Sameshima, Y. Nigara, J. Mizusaki, *Solid State Ionics* **1999**, *125*, 325.
[41] J. Nowotny, T. Norby, T. Bak, *J. Phys. Chem. C* **2010**, *114*, 18215.
[42] E. V. Lavrov, *Physica B* **2003**, *340*, 195.
[43] R. Waser, R. Dittmann, G. Staikov, K. Szot, *Adv. Mater.* **2009**, *21*, 2632.
[44] J. J. Yang, M. D. Pickett, X. M. Li, D. A. A. Ohlberg, D. R. Stewart, R. S. Williams, *Nat. Nanotechnol.* **2008**, *3*, 429.
[45] A. Janotti, C. G. van der Walle, *Phys. Rev. B* **2007**, *76*, 165202.
[46] H. L. Lein, K. Wiik, T. Grande, *Solid State Ionics* **2006**, *117*, 1587.
[47] J. I. Jung, D. D. Edwards, *J. Eur. Ceram. Soc.* **2012**, *32*, 3733.
[48] M. Y. Oh, A. Unemoto, K. Amezawa, T. Kawada, *J. Electrochem. Soc.* **2012**, *159*, F659.
[49] J. Maier, *Physcial Chemistry of Ionic Materials*, Wiley, Chichester **2004**.
[50] J. Claus, M. Leonhardt, J. Maier, *J. Phys. Chem. Sol.* **2000**, *61*, 1199.
[51] J. H. Yu, J.-S. Lee, J. Maier, *Phys. Chem. Chem. Phys.* **2005**, *7*, 3560.
[52] L. Wang, R. Merkle, J. Maier, *J. Electrochem. Soc.* **2010**, *157*, B1802.
[53] J. I. Jung, S. T. Misture, D. D. Edwards, *Solid State Ionics* **2010**, *181*, 1287.
[54] J. Martynczuk, K. Efimov, L. Robben, A. Feldhoff, *J. Membr. Sci.* **2009**, *344*, 62.